Tropical cyclone integrated kinetic energy in an ensemble of HighResMIP simulations

Article

Accepted Version

Kreussler, P. ORCID: https://orcid.org/0000-0003-4328-4712, Caron, L.-P. ORCID: https://orcid.org/0000-0001-5221-0147, Wild, S. ORCID: https://orcid.org/0000-0002-1089-5579, Tomas, S. L., Chauvin, F. ORCID: https://orcid.org/0000-0001-6071-7212, Moine, M.-P., Roberts, M. J., Ruprich-Robert, Y., Seddon, J. ORCID: https://orcid.org/0000-0003-1302-1049, Valcke, S. ORCID: https://orcid.org/0000-0002-0438-5978, Vannière, B. and Vidale, P. L. ORCID: https://orcid.org/0000-0002-1800-8460 (2021) Tropical cyclone integrated kinetic energy in an ensemble of HighResMIP simulations. Geophysical Research Letters, 48 (5). e2020GL090963. ISSN 1944-8007 doi: https://doi.org/10.1029/2020gl090963 Available at https://centaur.reading.ac.uk/96719/

It is advisable to refer to the publisher's version if you intend to cite from the work. See Guidance on citing.

To link to this article DOI: http://dx.doi.org/10.1029/2020gl090963

www.reading.ac.uk/centaur

CentAUR

Central Archive at the University of Reading

Reading's research outputs online

Tropical Cyclone Precipitation in the HighResMIP Atmosphere-only Experiments of the PRIMAVERA Project

Wei Zhang[1,2*], Gabriele Villarini[1], Enrico Scoccimarro[3], Malcolm Roberts[4], Pier Luigi Vidale[5], Benoıt Vanniere[5], Louis-Philippe Caron[6], Dian Putrasahan[7], Christopher Roberts[8], Retish Senan[8], and Marie-Pierre Moine[9]

[1] IIHR-Hydroscience & Engineering, The University of Iowa, Iowa City, Iowa, USA

[2] Department of Plants, Soils and Climate, Utah State University, Utah, USA

[3] Fondazione Centro Euro-Mediterraneo sui Cambiamenti Climatici, Bologna, Italy

[4] UK Meteorological Office, Exeter, UK

[5] National Centre for Atmospheric Science (NCAS), Department of Meteorology, University of Reading, Reading, UK

[6] Barcelona Supercomputing Center (BSC), Barcelona, Spain

[7] Max Planck Gesellschaft zur Foerderung der Wissenschaften E.V. (MPI-M), Hamburg, Germany

[8] European Centre for Medium-Range Weather Forecasts (ECMWF), Reading, UK

[9] Climat, Environnement, Couplages, Incertitudes (CECI), Universit´e de Toulouse, CNRS, Cerfacs, Toulouse, France

Revision submitted to

Climate Dynamics

*Corresponding author:

Wei Zhang, Ph.D.
Department of Plants, Soils and Climate, Utah State University, Utah, USA.
Email: w.zhang@usu.edu
Phone: (435) 791-1101

32   Abstract

33   This study examines the climatology and structure of rainfall associated with tropical cyclones

34   (TCs) based on the atmosphere-only Coupled Model Intercomparison Project Phase 6 (CMIP6)

35   HighResMIP runs of the PRocess-based climate sIMulation: AdVances in high resolution

36   modelling and European climate Risk Assessment (PRIMAVERA) Project during 1979-2014.

37   We evaluate how the spatial resolution of climate models with a variety of dynamic cores and

38   parameterization schemes affects the representation of TC rainfall. These HighResMIP

39   atmosphere-only runs that prescribe historical sea surface temperatures and radiative forcings

40   can well reproduce the observed spatial pattern of TC rainfall climatology, with high-resolution

41   models generally performing better than the low-resolution ones. Overall, the HighResMIP

42   atmosphere-only runs can also reproduce the observed percentage contribution of TC rainfall to

43   total amounts, with an overall better performance by the high-resolution models. The models

44   perform better over ocean than over land in simulating climatological total TC rainfall, TC

45   rainfall proportion and TC rainfall per TC in terms of spatial correlation. All the models in the

46   HighResMIP atmosphere-only runs underestimate the observed composite TC rainfall structure

47   over both land and ocean, especially in their lower resolutions. The underestimation of rainfall

48   composites by the HighResMIP atmosphere-only runs is also supported by the radial profile of

49   TC rainfall. Overall, the increased spatial resolution generally leads to an improved model

50   performance in reproducing the observed TC rainfall properties.

51

2

1. Introduction

Tropical cyclones (TCs) are associated with extreme rainfall and are responsible for extensive damages and numerous fatalities (e.g., Peduzzi et al. 2012; Rappaport 2014; Czajkowski et al. 2017; Klotzbach et al. 2018; Bosma et al. 2020). For example, Hurricanes Harvey and Florence serve to highlight the catastrophes that could be caused by extreme TC rainfall (e.g., Emanuel 2017; Reed et al. 2018; Risser and Wehner 2017; Van Oldenborgh et al. 2017; Wang et al. 2018; Zhang et al. 2018) and are just two recent examples of a long list of catastrophic events. According to the National Oceanic and Atmospheric Administration (NOAA) National Center for Environmental Information (NCEI) (2020), there have been 44 TCs affecting the United States causing damage in excess of one billion dollars between 1980 and 2019; in total, these events caused $945.9B (Consumer Price Index-Adjusted) and 6,502 fatalities.

Rainfall associated with TCs tends to be larger than for non-TC events. For instance, within the novel statistical framework of the Metastatistical Extreme Value Distribution, Miniussi et al. (2020) showed that the distribution of TC rainfall is different from the non-TC rainfall in the Eastern United States, especially for multi-day events, and that these storms tend to result in larger rainfall values. The impact of the TC rainfall is remarkable not only along the coastline, but also hundreds of miles inland in terms of flooding (e.g., Villarini et al. 2014a; Khouakhi et al. 2017; Aryal et al. 2018) and landslides (e.g., Bucknam et al. 2001). Despite these negative effects, they can also bring water critical for groundwater recharge, water supply and drought mitigation (e.g., Abdalla and Al-Abri 2011; Kam et al. 2013; Zhang et al. 2017). It is therefore crucial that we improve our understanding of the processes and characteristics of TC rainfall, which could in turn lead to an improvement in its simulation and seasonal forecasting (e.g., Barlow 2011; Luitel et al.

74 2018; Liu et al. 2019; Prat and Nelson, 2016; Touma et al. 2019; Vecchi et al. 2019; Zhang et al.

75 2019).

76   There are several drivers controlling TC rainfall, including low-level vertical wind shear

77 (Corbosiero and Molinari 2003; Tang et al. 2014), terrain effects (DeHart and Houze Jr 2017;

78 Nguyen et al. 2017), TC structure (Chen et al. 2006; Hence and Houze Jr 2012; Yu et al. 2017),

79 sea surface temperature (Langousis and Veneziano 2009; Lin et al. 2015), and atmospheric

80 aerosols (Wang et al. 2014; Zhao et al. 2018). Over the years and thanks to advances in observing

81 capabilities, major progress has been made in understanding the temporal and spatial components

82 of TC rainfall through satellite monitoring (e.g., Rios Gaona et al. 2018; Jiang and Zipser 2010;

83 Jiang et al. 2011; Prat and Nelson 2013b), radar data (e.g., Villarini et al. 2011; Bao et al. 2017;

84 Janapati et al. 2020) and rain gauges (e.g., Khouakhi et al. 2017; Villarini and Denniston 2016).

85 Overall, these studies indicate that TC rainfall substantially contributes to the mean and extreme

86 precipitation events, particularly along coastal regions (Khouakhi et al. 2017; Shepherd et al. 2007;

87 Knight et al. 2009; Prat et al. 2013; Villarini et al. 2011; 2014b). In addition to observations,

88 numerical models with the capability of resolving TCs have been used to examine TC rainfall (e.g.,

89 Daloz et al. 2010; Kim et al. 2018; Liu et al. 2018; 2019; Moon et al. 2020; Scoccimarro et al.

90 2014; 2017a; Villarini et al. 2014; Zhang et al. 2019). While climate models can well simulate the

91 overall climatology of TC rainfall (e.g., Zhang et al. 2019), these models have limitations in

92 simulating individual events and exhibit strong discrepancies in the simulated pattern and

93 magnitude of TC rainfall (Scoccimarro et al. 2017c; Wright et al. 2015; Zhang et al. 2019).

94   In the climate modeling community, special attention has been paid to the examination of

95 the impacts of horizontal resolution on TC simulations (e.g., Zhao et al. 2009; Caron et al. 2011;

96 Manganello et al. 2012; Wehner et al. 2014; Roberts et al. 2015; 2020; Murakami et al. 2015;

4

97   Zhang et al. 2015; Vecchi et al. 2019). Despite these efforts, it is difficult to generalize the

98   conclusions of these studies because of the differences in experimental design, tracking algorithm,

99   and model parameters. While much of the focus has been on the role of resolution in terms of TC

100   characteristics, recently Zhang et al. (2019) assessed the role of horizontal resolution of two

101   climate models (i.e., the Geophysical Fluid Dynamics Laboratory (GFDL) Forecast-Oriented Low

102   Ocean Resolution version of CM2.5 (FLOR, ~50km) and the High-Resolution FLOR (HiFLOR,

103   ~25km)) in simulating TC rainfall and found that the high-resolution model (~25km) outperforms

104   the low-resolution model (~50km) in reproducing and forecasting TC rainfall.

105   Based on this overview, numerical models have advanced our understanding of TC rainfall

106   and provided insights into future projection of TC rainfall; however, there is a very limited number

107   of climate models that can properly resolve TCs. Although there are individual studies that have

108   focused on the impacts of horizontal resolution on TCs, there are many differences in the models'

109   setups and simulations that would lead to the different behaviors in simulating TC rainfall,

110   representing a critical obstacle in terms of the generalization of the results from different studies.

111   Most conclusions drawn on the projection of TC rainfall are based on the fifth phase of the Coupled

112   Model Intercomparison Project (CMIP5)'s climate models with spatial resolution of ~1-3 degrees,

113   which are too coarse to properly resolve TCs. To overcome this limitation, the sixth phase of the

114   Coupled Model Intercomparison Project (CMIP6) High Resolution Model Intercomparison

115   Project (HighResMIP) provides multi-model and multi-resolution simulations to the scientific

116   community (Haarsma et al. 2016). Using the CMIP6 HighResMIP protocol, the European Union

117   Horizon 2020's PRocess-based climate sIMulation: AdVances in high resolution modelling and

118   European climate Risk Assessment (PRIMAVERA) project has contributed global atmospheric

119   general circulation models (AGCM) simulations at a CMIP6-type resolution (i.e., ~100 km) and

120 higher (e.g., ~25 km), which allow us to examine TCs and understand the robustness of changes

121 in TC rainfall across a wide range of numerical models and spatial resolutions (Roberts et al. 2020).

122 Roberts et al. (2020) examined the roles of horizonal resolution in simulating TCs in terms of

123 frequency, intensity, structure and accumulated cyclone energy across these models. In addition,

124 Vanniere et al. (2020) focused on the sensitivity of moisture budget associated with TC rainfall to

125 different spatial resolution of the climate models in this project. This study will take advantage of

126 the simulations archived in the PRIMAVERA project to evaluate the fidelity of these climate

127 models in representing TC rainfall and the dependence of skill on resolution.

128   The remainder of the manuscript is organized as follows. Section 2 describes data and

129 methods, followed by Section 3 that presents results based on observations and models. Finally,

130 Section 4 summarizes the main points and concludes the study.

131

132 **2. Data and Methods**

133   TC observations are obtained from the International Best Track Archive for Climate

134 Stewardship (IBTrACS) version 4 with longitude, latitude, time, intensity (i.e., maximum

135 sustained wind) and central pressure at the six-hour time scale (Knapp et al. 2010). Rainfall is

136 obtained from the Multi-Source Weighted-Ensemble Precipitation, version 2 (MSWEP V2) which

137 is a gridded precipitation dataset available during 1979–2017 with high spatial (0.1°) and temporal

138 (three-hour) resolution (Beck et al. 2017a,b). TC rainfall is defined as the rainfall at 6-hour

139 intervals within a 500-km radius of a TC center by accounting for the rainfall covering the inner

140 core of the TC and the adjacent rainbands (e.g., Dare et al. 2012; Villarini et al. 2014b; Zhang et

141 al. 2019). Although there might be some uncertainties in extracting TC rainfall using this radius at

142 each 6-hour time step, the selection of this radius is also supported by the fact that most

precipitation associated with TCs occurs within 5° (~500km) from the center of the storm for climate models (Trenberth et al. 2007; Vanniere et al. 2020). The TC-rainfall composites are the composites of the extracted TC rainfall using the 500-km radius and we process the TC rainfall for three scenarios: land and ocean, only land and only ocean.

We use the HighResMIP atmosphere-only simulations performed by the Met Office Hadley Centre's HadGEM3-GC313-GC31 (Roberts et al. 2019a), the European Centre for Medium-Range Weather Forecasts Integrated Forecasting System (ECMWF IFS) (Roberts et al. 2018), CNRM-CM6-1 developed by Centre National de Recherches Météorologiques—Groupe d'études de l'Atmosphère Météorologique/Centre Européen de Recherche et de Formation Avancée (Voldoire et al. 2019), the Fondazione Centro Euro-Mediterraneo sui Cambiamenti Climatici Climate Model Version 2 (CMCC-CM2-(V)HR4; Cherchi et al. 2019, Scoccimarro et al. 2020), the EC-EARTH3 Consortium's EC-Earth3P (Haarsma et al. 2019), and Max Planck Institute Earth System Model version 1.2 (MPI-ESM1-2; Gutjahr et al. 2019) (see Table 1 for details). The atmosphere-only HighResMIP experiments are forced by the historical estimates of sea surface temperature, sea ice, and radiative forcings (as described in Haarsma et al. 2016). It should be noted that the atmosphere-only HighResMIP simulations are slightly different from the CMIP6 (Eyring et al. 2016) AMIP experiments (Gates et al. 1999) in terms of forcing of aerosol, sea surface temperature and sea ice (Roberts et al. 2020). We obtain the model simulations archived in the Earth System Grid Federation (ESGF) nodes, including Roberts (HadGEM3-GC31; 2017a, 2017b, 2017c), Roberts et al. (ECMWF-IFS; 2017a, 2017b), Voldoire (CNRM-CM6-1; 2017, 2018), Scoccimarro et al. (CMCC-CM2-(V)HR4; 2017b, 2017c), EC-Earth Consortium (EC-Earth3P; 2018a, 2018b), and von Storch et al. (MPI-ESM1-2; 2017, 2019). In addition, the TC tracks obtained from these datasets are available from Roberts (2019b).

166   To facilitate the comparison of the simulation of TC rainfall, the climate model outputs are

167   grouped into high-, medium- and low- spatial-resolution models (Table 1). While ECMWF IFS

168   data provided to the HighResMIP simulations are based on a reduced-resolution regular grid, the

169   original ECMWF-IFS output uses the cubic octahedral reduced Gaussian grid, with resolutions of

170   Tco399 (~25 km) and Tco199 (~50 km) for the HR and LR configurations, respectively. Therefore,

171   we include ECMWF-IFS-HR/ECMWF-IFS-LR in the high-resolution/middle-resolution group,

172   respectively (Table 1). TC tracks with latitude, longitude, time and intensity are derived by

173   applying a tracker called "TRACK" to the simulations performed by these models (Hodges et al.

174   2017). This tracker uses the 6-hourly relative vorticity at the 850-, 700-, and 600-hPa levels for

175   tracking TCs and has been widely used in TC studies (Hodges et al. 2017).

176   We evaluate the performance of these models in simulating TC rainfall across the globe,

177   and for the basins (Table 2): western North Pacific, eastern North Pacific, North Atlantic, South

178   Atlantic, North Indian Ocean, South-West Indian Ocean and South Pacific & Australia. We use

179   spatial correlation and root mean square error (RMSE) as quantitative metrics for the evaluation.

180   Because there is no named storm in South Atlantic in observations during the study period (Table

181   S1), we do not include the analysis of spatial correlation and RMSE between observations and

182   models for this basin.

183   Beyond the high resolution of these models, a major advantage of the PRIMAVERA

184   Project is the consistency of the simulations and outputs: all the models were run using the same

185   forcings, and the tracking of the storms is the same across models, allowing for a direct comparison

186   in terms of model performance and on the role of resolution.

187

188   **3. Results**

3.1 Total TC rainfall

The annual total TC rainfall averaged over 1979-2014 in the observations exhibits regional differences across ocean basins (Figure 1). For example, the annual TC rainfall is the highest in the western North Pacific, followed by the eastern North Pacific. The annual TC rainfall in the North Atlantic is lower than in the eastern North Pacific and little TC rainfall is observed in the South Atlantic (Figure 1). Qualitatively, the climate models tend to capture the overall spatial climatological pattern of TC rainfall in the observations; this is particularly true in relation to the areas in the North Pacific characterized by larger TC rainfall values compared to the rest of the basins (Figure 2). The GCMs generally produce spurious TC rainfall in the South Atlantic (Figure 2). Specifically, CMCC-CM2-VHR4, EC-Earth3P-HR, ECMWF-IFS-HR, and ECMWF-IFS-LR reproduce well the total TC rainfall amount across different basins (Figure 2), consistent with spatial correlation and RMSE between observed and simulated total TC rainfall (Tables 3-4). In addition, CNRM-CM6-1-HR, CNRM-CM6-1, HadGEM3-GC31-HM, HadGEM3-GC31-MM, HadGEM3-GC31-LM point to an overestimation of the total TC rainfall, while EC-Earth3P, MPIESM1-2-XR and MPIESM1-2-HR to an underestimation of the total TC rainfall across all basins (Figure 2). This is consistent with the results of TC track density (Figure 3), which is also documented in Roberts et al. (2020) which reported that EC-Earth3P and MPIESM1-2-XR underestimate TC track density. Vanniere et al. (2020) also found that TC activity/frequency plays an important role in explaining the differences in total TC rainfall between high-resolution and low-resolution models. Based on the above results, high-resolution models tend to perform better in reproducing the observed climatology of TC rainfall. Overall, increase in model resolution tends to produce a higher amount of total TC rainfall for the CMCC models, EC-Earth3P models, HadGEM3-GC31 (i.e., HadEM3-GC31-HM and HadGEM3-GC31-LM) and ECMWF-IFS

9

212   models, while TC rainfall shows little to no sensitivity to spatial resolution in CNRM-CM6-1 and

213   MPIESM1-2 models (Figure 2). Four of the six models exhibit remarkable differences in TC

214   rainfall between high-resolution and low-resolution models while the other two show similar

215   results (Figure 2). The low sensitivity to spatial resolution in CNRM-CM6-1 and MPIESM1-2

216   models may be due to low absolute resolution in the models, the high-resolution version of which

217   is around ~50km (Table 1).

218   **3.2 Contribution of TC rainfall to Total Rainfall**

219   In addition to total TC rainfall, we also examine the percentage contribution of TC rainfall

220   to total rainfall. In the observations, the percentage contribution presents remarkable regional

221   differences with the highest values in the western and eastern North Pacific (Figure 4), consistent

222   with total TC rainfall (Figure 1). Climate models exhibit strong discrepancies in the capability of

223   reproducing the observed percentage contribution (Figure 4). Globally, EC-Earth3P-HR,

224   ECMWF-IFS-HR, ECMWF-IFS-LR, HadGEM3-GC31-HM, HadGEM3-GC31-MM, and

225   HadGEM3-GC31-LM reproduce well the observed contribution of TC rainfall in terms of RMSE.

226   CMCC-CM2-VHR4, EC-Earth3P-HR, EC-Earth3P, ECMWF-IFS-HR, ECMWF-IFS-LR, and

227   HadGEM3-GC31 models produce spatial correlations greater than 0.8, suggesting a good

228   performance (Table 5). The models exhibit marked regional differences. For example, CNRM-

229   CM6-1-HR and CNRM-CM6-1 reproduce well the observed contribution of TC rainfall in the

230   western North Pacific, and the performance of these models is not very promising in the North

231   Indian Ocean (Figure 4 and Tables 5-6). High-resolution models generate a higher contribution,

232   more similar to the observations except for MPIESM1-2-XR/MPIESM1-2-HR and CNRM-CM6-

233   1-HR/CNRM-CM6-1, which produce similar percentage contributions between high-resolution

234   and low-resolution models (Figure 4). Therefore, most of the high-resolution models perform

235 better than their low-resolution counterparts in reproducing the global fractional contribution

236 (Figure 4 and Table 5). To further understand the proportion of TC rainfall, we also examine the

237 bias in the models (Figure 5). Overall, the bias in TCR proportion (Figure 5) is mainly due to the

238 bias in TC rainfall (Figure 2), rather than total precipitation (Figure 6).

239 **3.3 TC rainfall per track density**

240   All the models in the PRIMAVERA Project underestimate the amount of TC rainfall per

241 track density (i.e., total TC rainfall divided by track density) in the observations (Figure 7).

242 Therefore, given that the TC rainfall amounts identified in the models were similar to the

243 observations, it means that there are generally more storms in the models than in the observational

244 records. As we compare the results between the different resolutions of the models, some models

245 (i.e., CMCC-CM2, CNRM and HadGEM3-GC31) have a tendency for lower-resolution versions

246 to have larger per-TC rainfall amounts. This counter-intuitive results may be due to the fact that

247 lower TC density is produced by low-resolution simulations than in the high-resolution ones

248 (Figure 3), consistent with Vanniere et al. (2020) showing that rainfall per TC is biased high in

249 low-resolution models. The spatial correlation between observed and simulated amount of TC

250 rainfall per track density (Table S2) is lower than for total TC rainfall or fractional contribution,

251 with most of the correlation coefficients that are not statistically significant. Among the models

252 used in this study, the CNRM models perform the best in simulating the rainfall per track density

253 (Figure 7 and Tables S2-3) and this is consistent with the fact that CNRM performs well in

254 simulating the strongest TCs (Roberts et al. 2020).

255 **3.4 TC rainfall over Ocean and Land**

256   We also evaluate the performance of the models in simulating climatological TC rainfall

257 over ocean and land. Overall, the models perform better in simulating total TC rainfall, TC rainfall

258   proportion and TC rainfall per TC over ocean than over land in terms of spatial correlation (Tables

259   S4-6). However, the models generate a larger RMSE for the three metrics over ocean than over

260   land (Tables S4-6), and this may be due to a large climatology of TC rainfall over ocean (Figure

261   1).

3.5 Composites and Profile of TC rainfall

263   We process the composite TC rainfall (within the 500-km radius of TC center) at 6-hour

264   time step for all the storms, those in the northern hemisphere and those in the southern hemisphere

265   in observations and climate models (Figure 8). The composite TC rainfall (within the 500-km

266   radius) at 6-hourly intervals in the observations is higher than model simulations over ocean and

267   land (Figure 8). CMCC-CM2-VHR4 performs the best in reproducing the composite TC rainfall

268   over ocean and land, with larger precipitation values closer to the center of circulation of the

269   storms, even though the size of the TCs tends to be smaller than in the observations and in other

270   models (e.g., CNRM). There is also a tendency for the storms in the northern hemisphere to exhibit

271   larger rainfall values compared to those in the southern hemisphere, consistent with the

272   observations. The high-resolution models produce larger composite TC rainfall rate than low-

273   resolution models, which tend to spread rainfall over larger distances from the center of circulation

274   of the TCs (Figure 8). In addition, we compare the composite rainfall in the 200 strongest storms

275   in observations and the low- and high-resolution models. Overall, the composite rainfall rate in the

276   high-resolution models is larger than in the low-resolution ones except for the MPI-ESM 1-2

277   models that simulate similar composite TC rainfall (Figure 9). The differences in composite TC

278   rainfall of the 200 strongest TCs between low-resolution and high-resolution models (Figure 9)

279   are more remarkable than the results for all TCs (Figure 8), and this may be due to a large portion

280   of intense TCs in the high-resolution models than low-resolution ones (Roberts et al. 2020). To

281 assess whether the models' skill is different in simulating TC rainfall over ocean or land mass, we

282 examine the composite TC rainfall over ocean and land, separately. The composite TC rainfall

283 over the ocean exhibits similar characteristics as those over land & ocean, with a well-defined

284 center of circulation, albeit presenting a slightly higher magnitude (Figure 10). While almost all

285 the models underestimate the composite TC rainfall over land compared with observations (Figure

286 11), CMCC-CM2-VHR4 slightly overestimates the center of composite TC rainfall over land and

287 HadGEM3-GC31-HM produces a similar magnitude of composite TC rainfall over land (Figure

288 11). Given the fact that TCs in models have a shorter path on land than the observations (due to

289 the tracker) and TC rainfall rate over ocean is larger than over land, this suggests that the

290 underestimation of composite TC rainfall in models might be even more pronounced than the

291 results here. Based on these results, there are no large differences in the performance of the models

292 in reproducing composite TC rainfall over ocean or land. Note that the composite rainfall patterns

293 are consistent with the results in Kim et al. (2018) which examined the composite TC rainfall

294 across a family of Geophysical Fluid Dynamics Laboratory (GFDL) models.

295   In addition to the examination of the composite TC rainfall, we compute the radial profile

296 of TC rainfall across different models grouped by spatial resolution (Table 1) and land/ocean

297 masks (Figure 12). Consistent with the results in Figures 8-11, the observed rainfall tends to be

298 higher than what is generated by these models, especially closer to their center of circulation; this

299 statement is valid regardless of resolution, and whether over land or ocean. The observed TC

300 rainfall over the oceans tends to peak within 100 km from the center of the storm, and then to

301 rapidly decrease as we move further away. This feature is generally well captured by the models,

302 with the CMCC-CM2-VHR4 tending to perform the best among high-resolution groups. Among

303 the mid-resolution group, HadGEM3-GC31-MM exhibits the highest skill in simulating the radial

304   profile of TC rainfall, while CNRM-CM6-1 tends to perform the best among the low-resolution

305   group (Figure 12). The model performance in terms of TC rainfall when the storms are over land

306   is similar to that mentioned for the storms over the ocean, even though the rainfall amounts tend

307   to be smaller and to decrease more slowly as they progress inland. The radial profile of TC rainfall

308   is consistent with Kim et al. (2018) and Moon et al. (2020) in terms of pattern and magnitude of

309   TC rainfall across different climate models.

310

311   **4. Conclusion**

312   TC rainfall has been a challenge for climate modeling community because this metric is

313   associated with TC genesis, track, and intensity. By taking advantage of the European Union

314   Horizon 2020's PRIMAVERA Project, we have examined the skill of state-of-the-art global

315   climate models in reproducing several aspects of the rainfall associated with these storms in

316   HighResMIP atmosphere-only experiments and assessed the dependence of the skill on model

317   resolution.

318   In general, high-resolution models perform better than their lower resolution counterparts

319   in reproducing several characteristics of the TC distribution. They tend to provide a more realistic

320   representation of the observations both in terms of patterns and amounts, except for average TC

321   rainfall per track density for which low-resolution models seem better for some models. The

322   simulation of TC rainfall by these models exhibits remarkable regional differences and

323   discrepancies. For example, the CMCC-CM2 and ECMWF-IFS models reproduce the total TC

324   rainfall found in observations, while they slightly underestimate their percentage contribution and

325   overall amount per track density. By contrast, CNRM-CM6-1 and HadGEM3-GC31 models

326   overestimate total TC rainfall, but they reproduce the fractional contribution of TC rainfall to total

327   rainfall. MPIESM1-2 and EC-Earth3P models underestimate most of the metrics associated with

328   TC rainfall. Overall, the models perform better in simulating climatological total TC rainfall, TC

329   rainfall proportion and TC rainfall per TC over ocean than over land in terms of spatial correlation.

330   However, the models generate larger RMSE for the three metrics over ocean than over land,

331   probably due to a larger climatology of TC rainfall over ocean.

332   When we stratified the results of composite TC rainfall across land and ocean, we did not

333   find any large changes in performance of these models, as they were able to reproduce the overall

334   patterns albeit with lower rainfall magnitudes. Overall, CMCC-CM2-VHR4 performs the best in

335   simulating the radial profile of TC rainfall among the high-resolution model group, while

336   HadGEM3-GC31-MM (CNRM-CM6-1) exhibits the highest skill in simulating the radial profile

337   of TC rainfall in the mid-resolution (low-resolution) group.

338   While most models tend to improve their performance as we increase their horizontal

339   resolution, the CNRM-CM6-1 and MPIESM1-2 models are two exceptions, producing similar

340   results in their low- and high- resolution versions. Such similar performances between high-

341   resolution and low-resolution climate models need to be further investigated from the perspective

342   of convection, circulation and TC dynamics. For example, Vanniere et al (2020) investigated

343   possible mechanisms by examining moisture budget, and found that the distribution of

344   precipitation per TC averaged in a 5-degree radial cap does not change significantly, which can be

345   explained by the large-scale balance that shapes the moisture budget of TCs.

346   In summary, our findings indicate that the investment in performing the high-resolution

347   simulations with these models has been paid off in terms of the gained realism in reproducing TC

348   rainfall. As we increase the horizontal resolution and we improve the description of the processes

349   at play, we expect to further improve the simulation of these storms, providing basic information

350   towards our preparation, mitigation and response efforts.

351
352
353   **Acknowledgetments:**
354

360

Reference:

Abdalla, O., and R. bin Y. Al-Abri, (2011). Groundwater recharge in arid areas induced by tropical cyclones: lessons learned from Gonu 2007 in Sultanate of Oman. Environ Earth Sci, 63, 229–239. https://doi.org/10.1007/s12665-010-0688-y

Aryal, Y.N., G. Villarini, W. Zhang, and G.A. Vecchi, Long term changes in flooding and heavy rainfall associated with North Atlantic tropical cyclones: Roles of the North Atlantic Oscillation and El Niño-Southern Oscillation, Journal of Hydrology, 559, 698-710, 2018.

Bao, X., D. Wu, X. Lei, L. Ma, D. Wang, K. Zhao, and B. J.-D. Jou, 2017: Improving the extreme rainfall forecast of Typhoon Morakot (2009) by assimilating radar data from Taiwan Island and mainland China. *Journal of Meteorological Research*, **31,** 747-766.

Barlow, M., 2011: Influence of hurricane-related activity on North American extreme precipitation. Geophysical Research Letters, 38 , L04705.

Beck, H. E., A. I. Van Dijk, V. Levizzani, J. Schellekens, D. Gonzalez Miralles, B. Martens, and A. De Roo, 2017a: MSWEP: 3-hourly 0.25 global gridded precipitation (1979-2015) by merging gauge, satellite, and reanalysis data. *Hydrology and Earth System Sciences*, **21,** 589-615.

Bosma, C. D., D. B. Wright, P. Nguyen, J. P. Kossin, D. C. Herndon, and J. M. Shepherd, 2020: An intuitive metric to quantify and communicate tropical cyclone rainfall hazard. Bulletin of the American Meteorological Society, 101, E206-E220.

Beck, H. E., and Coauthors, 2017b: Global-scale evaluation of 22 precipitation datasets using gauge observations and hydrological modeling. *Hydrology and Earth System Sciences*, **21,** 6201.

Bucknam, R. C., J.A. Coe, M.M. Chavarria, J.W. Godt, A.C. Tarr, … , and M.L. Johnson (2001). Landslides triggered by Hurricane Mitch in Guatemala - Inventory and discussion. USGS Report Number 2001-443.

Caron, L-P, CG Jones and K Winger (2011) Impact of resolution and downscaling technique in simulating recent Atlantic tropical cyclone activity. Climate Dynamics, 5, 869-892. doi: 10.1007/s00382-010-0846-7.

Chavas, D. R., N. Lin, W. Dong, and Y. Lin (2016), Observed Tropical Cyclone Size Revisited, *Journal of Climate*, *29*(8), 2923-2939, doi:10.1175/jcli-d-15-0731.1.

Chen, S. S., J. A. Knaff, and F. D. Marks Jr, 2006: Effects of vertical wind shear and storm motion on tropical cyclone rainfall asymmetries deduced from TRMM. *Monthly Weather Review*, **134,** 3190-3208.

Cherchi, A., and Coauthors, 2019: Global Mean Climate and Main Patterns of Variability in the CMCC-CM2 Coupled Model. *Journal of Advances in Modeling Earth Systems*, **11,** 185-209.

Corbosiero, K. L., and J. Molinari, 2003: The relationship between storm motion, vertical wind shear, and convective asymmetries in tropical cyclones. *Journal of the Atmospheric Sciences*, **60,** 366-376.

Czajkowski, J., G. Villarini, M. Montgomery, E. Michel-Kerjan, and R. Goska, Assessing current and future freshwater flood risk from North Atlantic tropical cyclones via insurance claims, Scientific Reports, 7, 1-10, 2017.

Daloz, A. S., F. Chauvin, and F. Roux, 2010: Tropical cyclone rainfall in the observations, reanalysis and ARPEGE simulations in the North Atlantic Basin. Hurricanes and climate change, Springer, 57-79.

Dare, R. A., N. E. Davidson, and J. L. McBride, 2012: Tropical cyclone contribution to rainfall over Australia. *Monthly Weather Review*, **140,** 3606-3619.

DeHart, J. C., and R. A. Houze Jr, 2017: Orographic modification of precipitation processes in Hurricane Karl (2010). *Monthly Weather Review*, **145,** 4171-4186.

EC-Earth Consortium (EC-Earth), 2018a: EC-Earth-858 Consortium EC-Earth3P model output prepared for CMIP6 HighResMIP. Earth System Grid Federation. http://cera860 www.dkrz.de/WDCC/meta/CMIP6/CMIP6.HighResMIP.EC-Earth-Consortium.EC861Earth3P

EC-Earth Consortium (EC-Earth), 2018b: EC-Earth-Consortium EC-Earth3P-HR model output prepared for CMIP6 HighResMIP. Earth System Grid Federation. http://cera-www.dkrz.de/WDCC/meta/CMIP6/CMIP6.HighResMIP.EC-Earth-Consortium.EC-Earth3P-HR

Emanuel, K., 2017: Assessing the present and future probability of Hurricane Harvey's rainfall. *Proceedings of the National Academy of Sciences*, **114,** 12681-12684.

Gates, W. L., and Coauthors, 1999: An overview of the results of the Atmospheric Model Intercomparison Project (AMIP I). *Bulletin of the American Meteorological Society*, **80,** 29-56.

Gutjahr, O., and Coauthors, 2019: Max Planck Institute Earth System Model (MPI-ESM1.2) for the High-Resolution Model Intercomparison Project (HighResMIP). *Geosci. Model Dev.*, **12,** 3241-3281.

Haarsma, R. J., and Coauthors, 2016: High Resolution Model Intercomparison Project (HighResMIP v1.0) for CMIP6. *Geosci. Model Dev.*, **9,** 4185-4208.

Hence, D. A., and R. A. Houze Jr, 2012: Vertical structure of tropical cyclone rainbands as seen by the TRMM Precipitation Radar. *Journal of the atmospheric sciences*, **69,** 2644-2661.

Hodges, K., A. Cobb, and P. L. Vidale, 2017: How well are tropical cyclones represented in reanalysis datasets? *Journal of Climate*, **30,** 5243-5264.

Janapati, J., and Coauthors, 2020: Raindrop Size Distribution Characteristics of Indian and Pacific Ocean Tropical Cyclones Observed at India and Taiwan Sites. *Journal of the Meteorological Society of Japan. Ser. II.*

Jiang, H., and E. J. Zipser, 2010: Contribution of tropical cyclones to the global precipitation from eight seasons of TRMM data: Regional, seasonal, and interannual variations. *Journal of climate*, **23,** 1526-1543.

Jiang, H., C. Liu, and E. J. Zipser, 2011: A TRMM-based tropical cyclone cloud and precipitation feature database. *Journal of applied meteorology and climatology*, **50,** 1255-1274.

Kam, J, J. Sheffield, X. Yuan, and E. F. Wood, 2013: The Influence of Atlantic Tropical Cyclones on Drought over the Eastern US (1980-2007), J. Climate, 26 (10), 3067-3086.

Kim, D., and Coauthors, 2018: Process-oriented diagnosis of tropical cyclones in high-resolution GCMs. *Journal of Climate*, 31, 1685-1702.

Khouakhi, A., G. Villarini, and G. A. Vecchi, 2017: Contribution of tropical cyclones to rainfall at the global scale. *Journal of Climate*, **30,** 359-372.

Klotzbach, P.J., S.G. Bowen, R. Pielke Jr., and M. Bell, Continental U.S. hurricane landfall frequency and associated damage: Observations and future risks, Bulletin of the American Meteorological Society, 99(7), 1359-1376, 2018.

Knapp, K. R., M. C. Kruk, D. H. Levinson, H. J. Diamond, and C. J. Neumann, 2010: The International Best Track Archive for Climate Stewardship (IBTrACS). *Bulletin of the American Meteorological Society*, **91,** 363-376.

452 Knight, D. B., and R. E. Davis, 2009: Contribution of tropical cyclones to extreme rainfall events
453   in the southeastern United States. *Journal of Geophysical Research: Atmospheres*, **114**.
454 Lin, Y., M. Zhao, and M. Zhang, 2015: Tropical cyclone rainfall area controlled by relative sea
455   surface temperature. *Nature communications*, **6,** 1-7.
456 Liu, M., G. A. Vecchi, J. A. Smith, and H. Murakami, 2018: Projection of landfalling–tropical
457   cyclone rainfall in the Eastern United States under anthropogenic warming. *Journal of*
458   *Climate*, **31,** 7269-7286.
459 Liu, M., G. A. Vecchi, J. A. Smith, and T. R. Knutson, 2019: Causes of large projected increases
460   in hurricane precipitation rates with global warming. *npj Climate and Atmospheric Science*,
461   **2,** 38.
462 Luitel, B., G. Villarini, and G.A. Vecchi, Verification of the skill of numerical weather
463   prediction models in forecasting rainfall from U.S. landfalling tropical cyclones, Journal of
464   Hydrology, 556, 1026-1037, 2018.
465 Manganello, J. V., and Coauthors, 2012: Tropical cyclone climatology in a 10-km global
466   atmospheric GCM: toward weather-resolving climate modeling. Journal of Climate, 25,
467   3867-3893.
468 Miniussi, A., G. Villarini, and M. Marani, Analyses through the metastatistical extreme value
469   distribution identify contributions of tropical cyclones to rainfall extremes in the eastern US,
470   Geophysical Research Letters, 47(7), e2020GL087238, 1-9, 2020.
471 Moon, Y., and Coauthors, 2020: Azimuthally averaged wind and thermodynamic structures of
472   tropical cyclones in global climate models and their sensitivity to horizontal resolution.
473   *Journal of Climate*, **33,** 1575-1595.
474 Murakami, H., and Coauthors, 2015: Simulation and prediction of category 4 and 5 hurricanes in
475   the high-resolution GFDL HiFLOR coupled climate model. Journal of Climate, 28, 9058-
476   9079.
477 Nguyen, L. T., R. F. Rogers, and P. D. Reasor, 2017: Thermodynamic and kinematic influences
478   on precipitation symmetry in sheared tropical cyclones: Bertha and Cristobal (2014). *Monthly*
479   *Weather Review*, **145,** 4423-4446.
480 NOAA National Centers for Environmental Information (NCEI) U.S. Billion-Dollar Weather
481   and Climate Disasters (2020). https://www.ncdc.noaa.gov/billions/, DOI: 10.25921/stkw-
482   7w73
483 Peduzzi, P., B. Chatenoux, H. Dao, A. De Bono, C. Herold, J. Kossin, F. Mouton, and O.
484   Nordbeck, Global trends in tropical cyclone risk, Nature Climate Change, 2, 289-294, 2012.
485 Prat, O. P., and B. R. Nelson, 2013a: Precipitation contribution of tropical cyclones in the
486   southeastern United States from 1998 to 2009 using TRMM satellite data. *Journal of*
487   *Climate*, **26,** 1047-1062.
488 ——, 2013b: Mapping the world's tropical cyclone rainfall contribution over land using the
489   TRMM Multi-satellite Precipitation Analysis. *Water Resources Research*, **49,** 7236-7254.
490 ——, 2016: On the link between tropical cyclones and daily rainfall extremes derived from
491   global satellite observations. Journal of Climate, 29, 6127-6135.
492 Rappaport, E.N., Fatalities in the United States from Atlantic tropical cyclones, 2014: New data
493   and interpretation, *Bulletin of the American Meteorological Society*, **95(3)**, 341-346.
494 Reed, K. A., A. Standfield, M. F. Wehner, and C. M. Zarzycki, 2018: The human influence on
495   Hurricane Florence. *website) accessed October*.
496 Rios Gaona, M.F., G. Villarini, W. Zhang, and G.A. Vecchi, The added value of IMERG in
497   characterizing rainfall in tropical cyclones, *Atmospheric Research*, 209, 95-102, 2018.

498 Risser, M. D., and M. F. Wehner, 2017: Attributable human-induced changes in the likelihood
499   and magnitude of the observed extreme precipitation during Hurricane Harvey. *Geophysical*
500   *Research Letters*, **44,** 12,457-412,464.
501 Roberts, C. D., R. Senan, F. Molteni, S. Boussetta, M. Mayer, and S. P. Keeley, 2018: Climate
502   model configurations of the ECMWF-Integrated Forecasting System (ECMWF-IFS cycle
503   43r1) for HighResMIP. *Geoscientific model development*, **11,** 3681-3712.
504 Roberts, C. D., R. Senan, F. Molteni, S. Boussetta, S. Keeley, 2017a: ECMWF ECMWF-IFS-LR
505   model output prepared for CMIP6 HighResMIP. Version 20170915.Earth System Grid
506   Federation. https://doi.org/10.22033/ESGF/CMIP6.2463
507 Roberts, C. D., R. Senan, F. Molteni, S. Boussetta, S. Keeley, 2017b: ECMWF ECMWF-IFS-
508   HR model output prepared for CMIP6 HighResMIP. Version 20170915.Earth System Grid
509   Federation. https://doi.org/10.22033/ESGF/CMIP6.2461
510 Roberts, M. J., and Coauthors, 2015: Tropical cyclones in the UPSCALE ensemble of high-
511   resolution global climate models. Journal of Climate, 28, 574-596.
512 Roberts, M., 2017a: MOHC HadGEM3-GC31-LM model o 1008 utput prepared for CMIP6
513   HighResMIP. Version 20170906.Earth System Grid Federation.
514   https://doi.org/10.22033/ESGF/CMIP6.1321
515 Roberts, M., 2017b: MOHC HadGEM3-GC31-MM model output prepared for CMIP6
516   HighResMIP. Version 20180818.Earth System Grid Federation.
517   https://doi.org/10.22033/ESGF/CMIP6.1902
518 Roberts, M., 2017c: MOHC HadGEM3-GC31-HM model output prepared for CMIP6
519   HighResMIP. Version 20170831.Earth System Grid
520   Federation.https://doi.org/10.22033/ESGF/CMIP6.446
521 Roberts, M. J., and Coauthors, 2019a: Description of the resolution hierarchy of the global
522   coupled HadGEM3-GC313-GC3.1 model as used in CMIP6 HighResMIP experiments.
523   *Geosci. Model Dev.*, **12,** 4999-5028.
524 Roberts, M. J., 2019b: CMIP6 HighResMIP: Tropical storm tracks as calculated by the TRACK
525   algorithm. Centre for Environmental Data Analysis, 2019.
526   http://catalogue.ceda.ac.uk/uuid/0b42715a7a804290afa9b7e31f5d7753
527 Roberts, M. J., and Coauthors, 2020: Impact of model resolution on tropical cyclone simulation
528   using the HighResMIP-PRIMAVERA multi-model ensemble. *Journal of Climate*, **33**, 2557-
529   2583.
530 Scoccimarro, E., S. Gualdi, G. Villarini, G. A. Vecchi, M. Zhao, K. Walsh, and A. Navarra,
531   2014: Intense precipitation events associated with landfalling tropical cyclones in response to
532   a warmer climate and increased CO2. *Journal of climate*, **27,** 4642-4654.
533 Scoccimarro, E., A. Bellucci, D. Peano, 2017a: CMCC CMCC-CM2-HR4 model output
534   prepared for CMIP6 HighResMIP. Version YYYYMMDD[1].Earth System Grid Federation.
535   https://doi.org/10.22033/ESGF/CMIP6.1359
536 Scoccimarro, E., A. Bellucci, D. Peano, 2017b: CMCC CMCC-CM2-VHR4 model output
537   prepared for CMIP6 HighResMIP. Version YYYYMMDD[1].Earth System Grid Federation.
538   https://doi.org/10.22033/ESGF/CMIP6.1367
539 Scoccimarro, E., G. Villarini, S. Gualdi, A. Navarra, G. Vecchi, K. Walsh, and M. Zhao, 2017c:
540   Tropical cyclone rainfall changes in a warmer climate. *Hurricanes and Climate Change*,
541   Springer, 243-255.

542 Scoccimarro E., Gualdi S., Bellucci A. , Peano D., Cherchi A., Vecchi G.A. , Navarra A. 2020:
543   The typhoon-induced drying of the Maritime Continent. PNAS doi:
544   10.1073/pnas.1915364117.
545 Shepherd, J. M., A. Grundstein, and T. L. Mote, 2007: Quantifying the contribution of tropical
546   cyclones to extreme rainfall along the coastal southeastern United States. *Geophysical*
547   *Research Letters*, **34**.
548 Tang, X., W.-C. Lee, and M. Bell, 2014: A squall-line-like principal rainband in Typhoon
549   Hagupit (2008) observed by airborne Doppler radar. *Journal of the Atmospheric Sciences*,
550   **71,** 2733-2746.
551 Taylor, K.E., D. Williamson and F. Zwiers, 2000: The sea surface temperature and sea ice
552   concentration boundary conditions for AMIP II simulations. In PCMDI Report 60, Program
553   for Climate Model Diagnosis and Intercomparison, Lawrence Livermore National
554   Laboratory, 25 pp.
555 Touma, D., S. Stevenson, S. J. Camargo, D. E. Horton, and N. S. Diffenbaugh, 2019: Variations
556   in the intensity and spatial extent of tropical cyclone precipitation. *Geophysical Research*
557   *Letters*, **46**, 13992-14002.
558 Van Oldenborgh, G. J., and Coauthors, 2017: Attribution of extreme rainfall from Hurricane
559   Harvey, August 2017. *Environmental Research Letters*, **12,** 124009.
560 Vecchi, G. A., and Coauthors, 2019: Tropical cyclone sensitivities to CO2 doubling: roles of
561   atmospheric resolution, synoptic variability and background climate changes. *Climate*
562   *Dynamics*, **53,** 5999-6033.
563 Villarini, G., J. A. Smith, M. L. Baeck, T. Marchok, and G. A. Vecchi, 2011: Characterization of
564   rainfall distribution and flooding associated with U.S. landfalling tropical cyclones: Analyses
565   of Hurricanes Frances, Ivan, and Jeanne (2004). *Journal of Geophysical Research:*
566   *Atmospheres*, **116**.
567 Villarini, G., R. Goska, J.A. Smith, and G.A. Vecchi, North Atlantic tropical cyclones and U.S.
568   flooding, Bulletin of the American Meteorological Society, 95(9), 1381-1388, 2014a.
569 Villarini, G., and R. F. Denniston, 2016: Contribution of tropical cyclones to extreme rainfall in
570   Australia. *International Journal of Climatology*, **36,** 1019-1025.
571 Villarini, G., and Coauthors, 2014b: Sensitivity of tropical cyclone rainfall to idealized global-
572   scale forcings. *Journal of climate*, **27,** 4622-4641.
573 Voldoire, A., and Coauthors, 2019: Evaluation of CMIP6 DECK Experiments With CNRM-
574   CM6-1. *Journal of Advances in Modeling Earth Systems*, **11,** 2177-2213.
575 Vanniere, B., and Coauthors, The moisture budget of tropical cyclones: large scale environmental
576   constraints and sensitivity to model horizontal resolution, Journal of Climate, 33, 8457-8474.
577 Voldoire, A., 2018: CNRM-CERFACS CNRM-1092 CM6-1 model output prepared for CMIP6
578   HighResMIP. Earth System Grid Federation.
579   http://cera1094www.dkrz.de/WDCC/meta/CMIP6/CMIP6.HighResMIP.CNRM-
580   CERFACS.CNRM1095CM6-1
581 Voldoire, A., 2017: CNRM-CERFACS CNRM-CM6-1-HR model output prepared for CMIP6
582   HighResMIP. Earth System Grid Federation.
583   http://cera1098www.dkrz.de/WDCC/meta/CMIP6/CMIP6.HighResMIP.CNRM-
584   CERFACS.CNRM1099CM6-1-HR
585 von Storch, J.-S., and Coauthors, 2017: MPI-M MPI-ESM1.2-HR model output prepared for
586   CMIP6 HighResMIP. Earth System Grid Federation.

587   http://cera1105www.dkrz.de/WDCC/meta/CMIP6/CMIP6.HighResMIP.MPI-M.MPI-ESM1-
588   2-HR
589 von Storch, J.-S., and Coauthors, 2019: MPI-M MPI-ESM1.2-XR model output prepared for
590   CMIP6 HighResMIP. Earth System Grid Federation.
591   http://cera1108www.dkrz.de/WDCC/meta/CMIP6/CMIP6.HighResMIP.MPI-M.MPI-ESM1-
592   2-XR
593 Wang, S. S., L. Zhao, J.-H. Yoon, P. Klotzbach, and R. R. Gillies, 2018: Quantitative attribution
594   of climate effects on Hurricane Harvey's extreme rainfall in Texas. *Environmental Research*
595   *Letters*, **13,** 054014.
596 Wang, Y., K.-H. Lee, Y. Lin, M. Levy, and R. Zhang, 2014: Distinct effects of anthropogenic
597   aerosols on tropical cyclones. *Nature Climate Change*, **4,** 368-373.
598 Wehner, M. F., and Coauthors, 2014: The effect of horizontal resolution on simulation quality in
599   the C ommunity A tmospheric M odel, CAM 5.1. Journal of Advances in Modeling Earth
600   Systems, 6, 980-997.
601 Wright, D. B., T. R. Knutson, and J. A. Smith, 2015: Regional climate model projections of
602   rainfall from US landfalling tropical cyclones. *Climate dynamics*, **45,** 3365-3379.
603 Yu, Z., Y. Wang, H. Xu, N. Davidson, Y. Chen, Y. Chen, and H. Yu, 2017: On the relationship
604   between intensity and rainfall distribution in tropical cyclones making landfall over China.
605   *Journal of Applied Meteorology and Climatology*, **56,** 2883-2901.
606 Zhang, M., X. Chen, M. Kumar, M. Marani, and M. Goralczyk (2017). Hurricanes and tropical
607   storms: A necessary evil to ensure water supply? Hydrological Processes, 31, 4414–4428.
608   https://doi.org/10.1002/hyp.11371
609 Zhang, W., and Coauthors, 2015: Improved Simulation of Tropical Cyclone Responses to ENSO
610   in the Western North Pacific in the High-Resolution GFDL HiFLOR Coupled Climate
611   Model. *Journal of Climate*, 29, 1391-1415.
612 Zhang, W., G. Villarini, G. A. Vecchi, and J. A. Smith, 2018: Urbanization exacerbated the
613   rainfall and flooding caused by hurricane Harvey in Houston. *Nature*, **563,** 384-388.
614 Zhang, W., G. Villarini, G. A. Vecchi, and H. Murakami, 2019: Rainfall from tropical cyclones:
615   high-resolution simulations and seasonal forecasts. *Climate Dynamics*, **52,** 5269-5289.
616 Zhao, C., Y. Lin, F. Wu, Y. Wang, Z. Li, D. Rosenfeld, and Y. Wang, 2018: Enlarging rainfall
617   area of tropical cyclones by atmospheric aerosols. Geophysical Research Letters, 45, 8604-
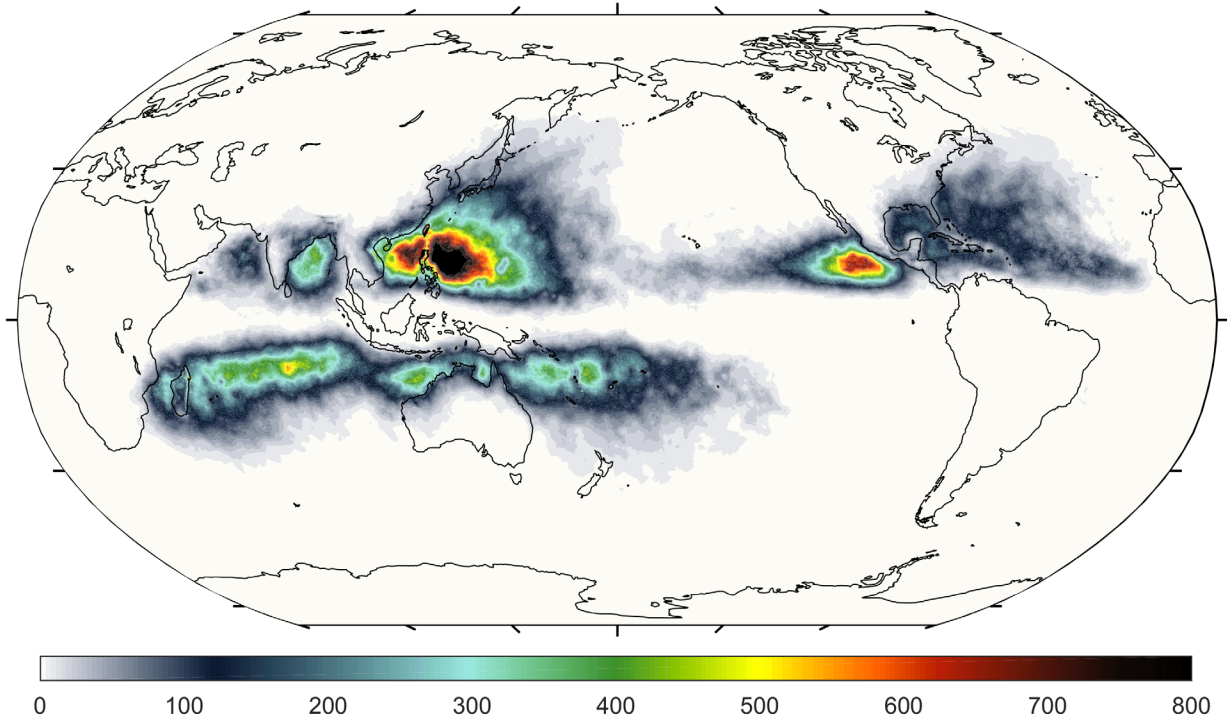618   8611.
619 Zhao, M., I. M. Held, S.-J. Lin, and G. A. Vecchi, 2009: Simulations of global hurricane
620   climatology, interannual variability, and response to global warming using a 50-km
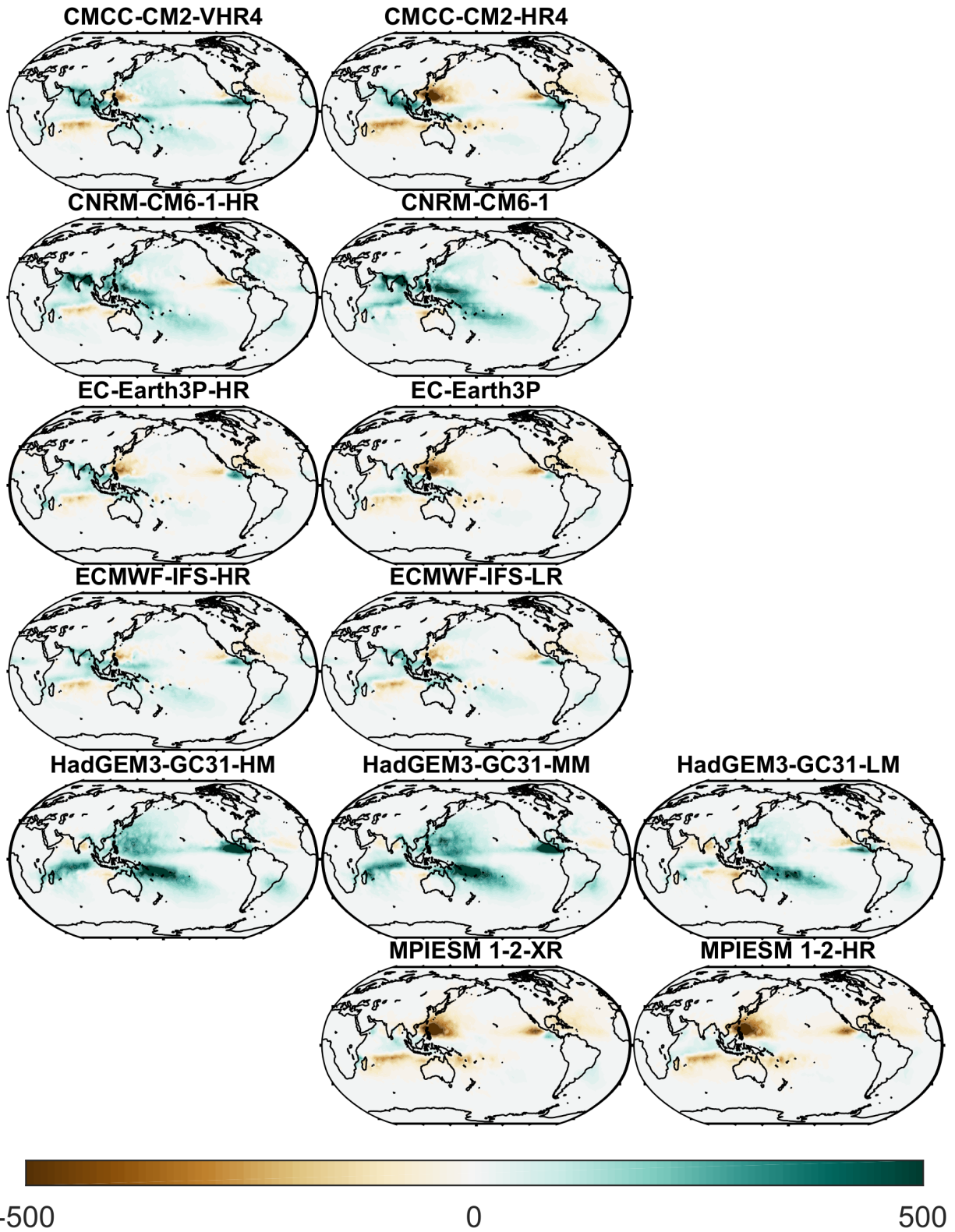621   resolution GCM. Journal of Climate, 22, 6653-6678.
622

623

624

625

626

627   Figure 1 Annual average TC rainfall (unit: mm/year) in observations.
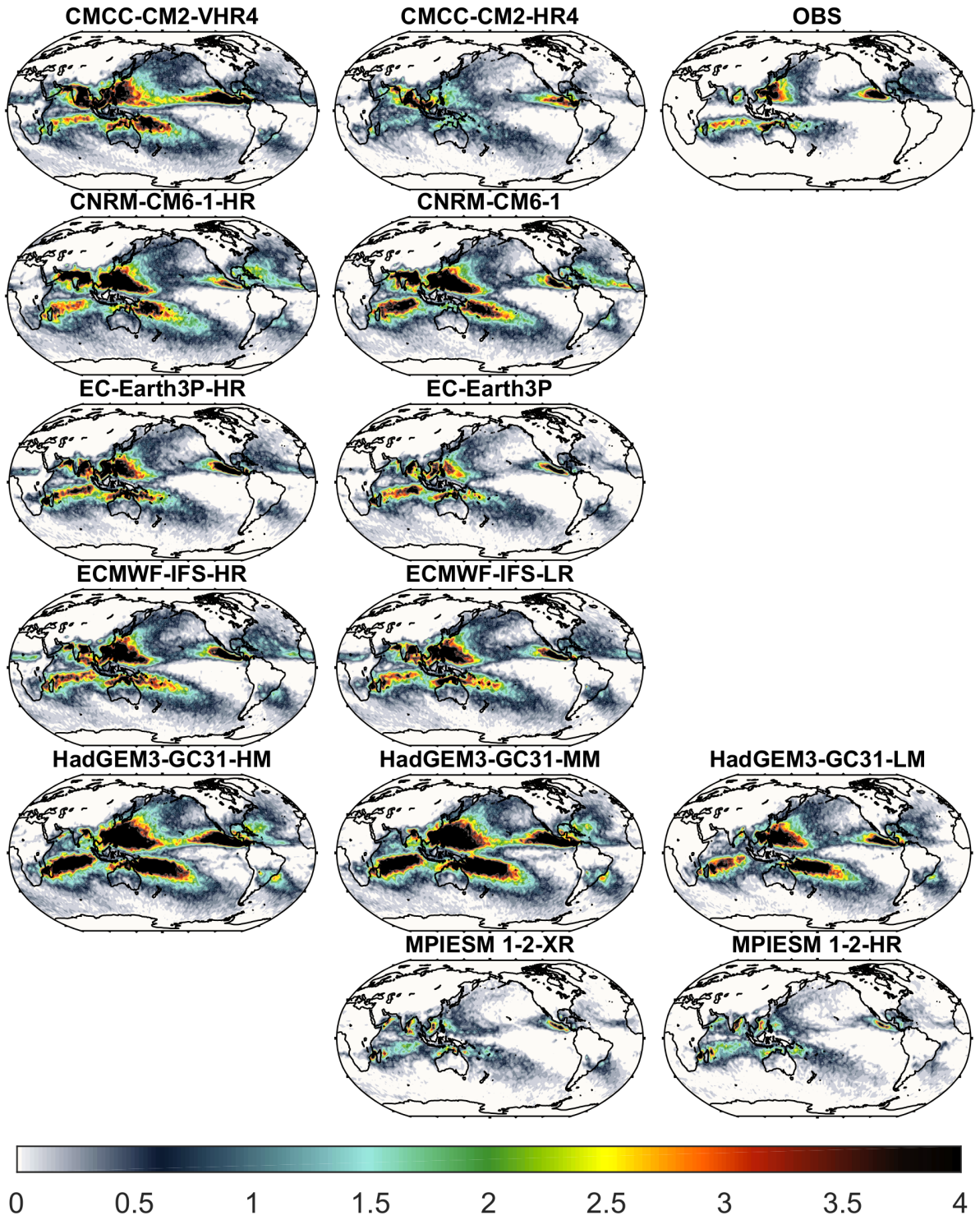
628

Figure 2. Differences in annual average TC rainfall (unit: mm/year) between observations and climate models archived in the PRIMAVERA Project (model minus observations).

632

Figure 3. Annual average TC track density obtained by binning TC tracks into 2×2 spatial boxes in observations and climate models archived in the PRIMAVERA Project.

633
634

635

636

637
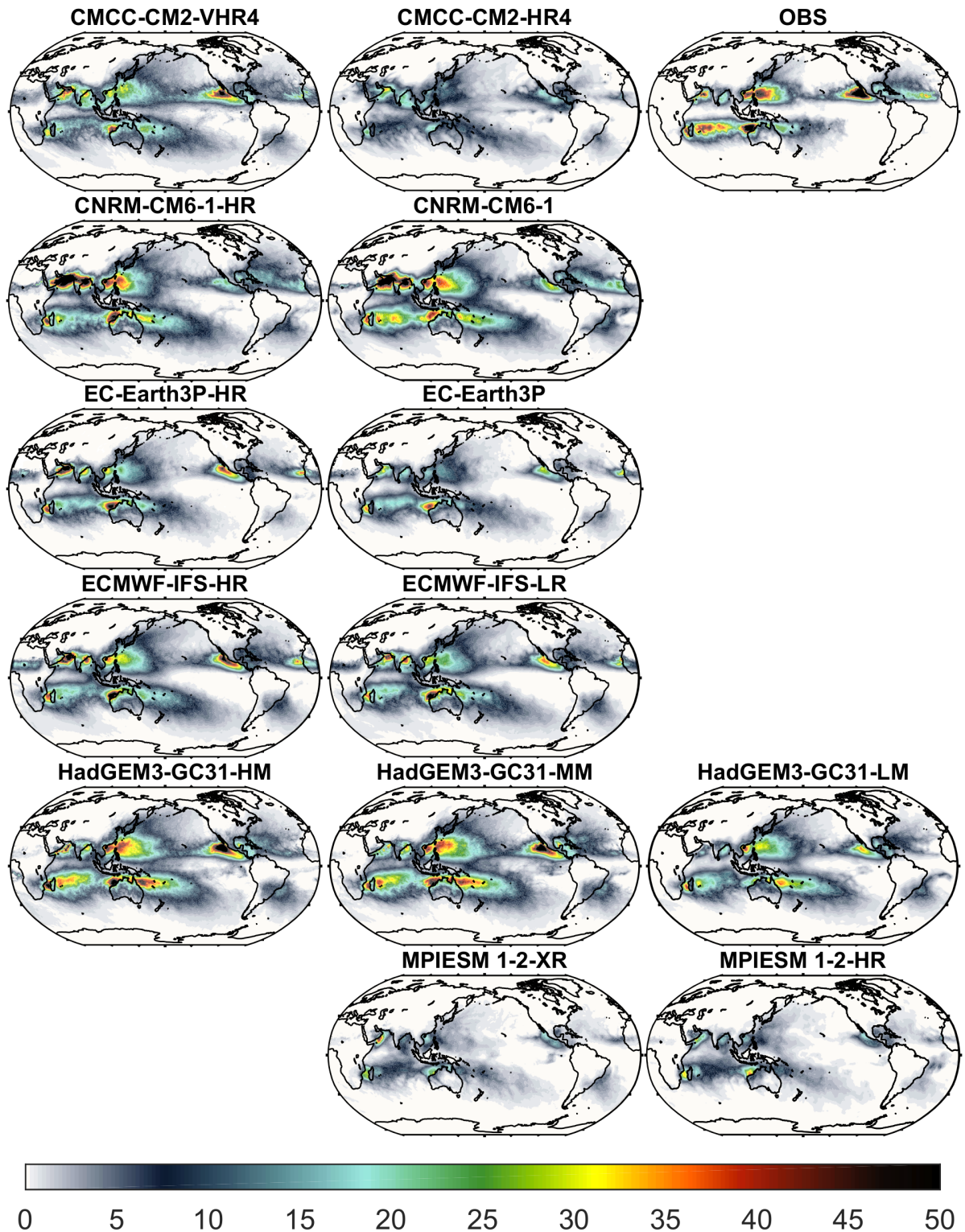
Figure 4. Percentage contribution of TC rainfall to total rainfall (unit: %) in observations and climate models archived in the PRIMAVERA Project.
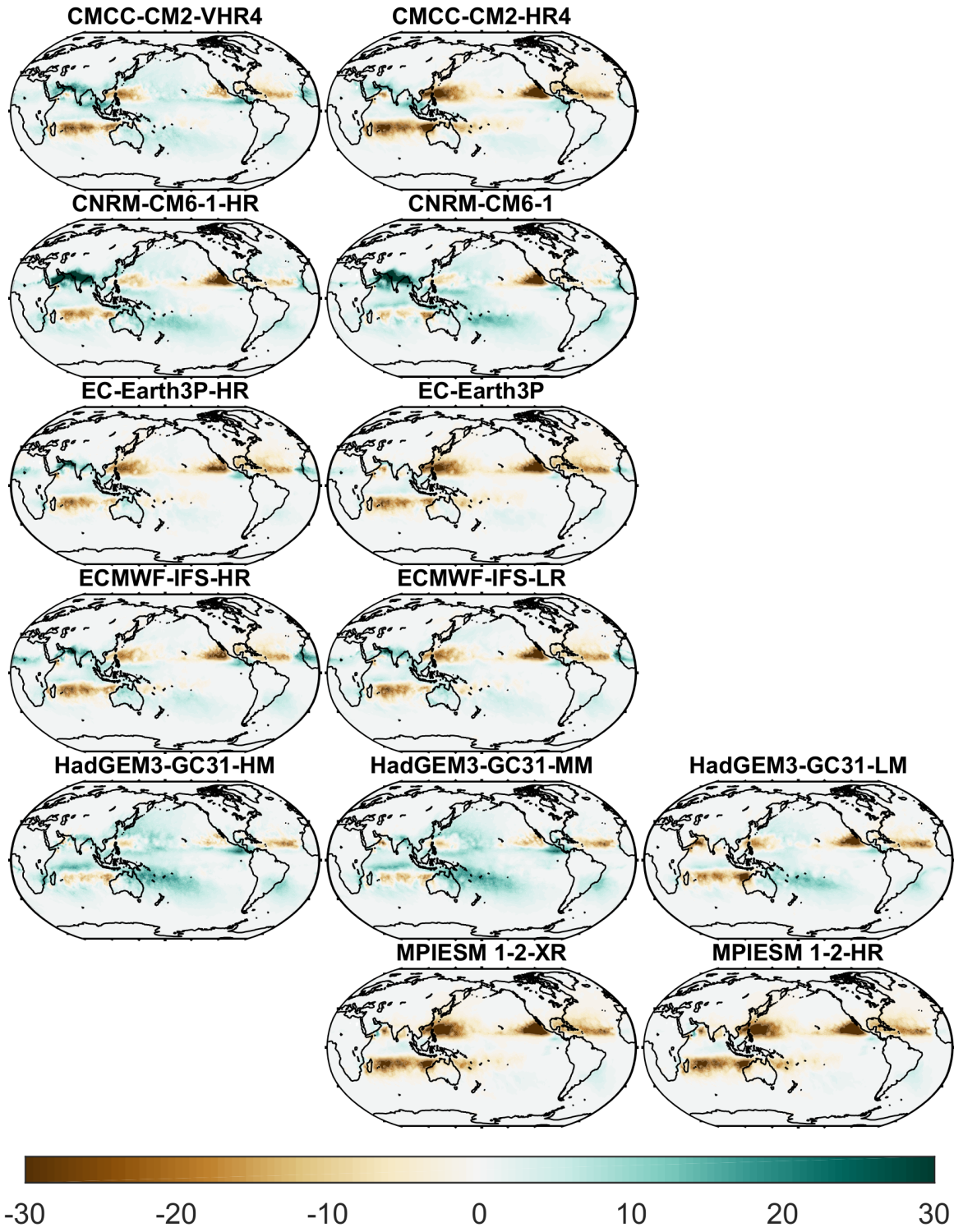
Figure 5. Bias (model minus observations) in the percentage contribution of TC rainfall to total rainfall (unit: %) in the models.
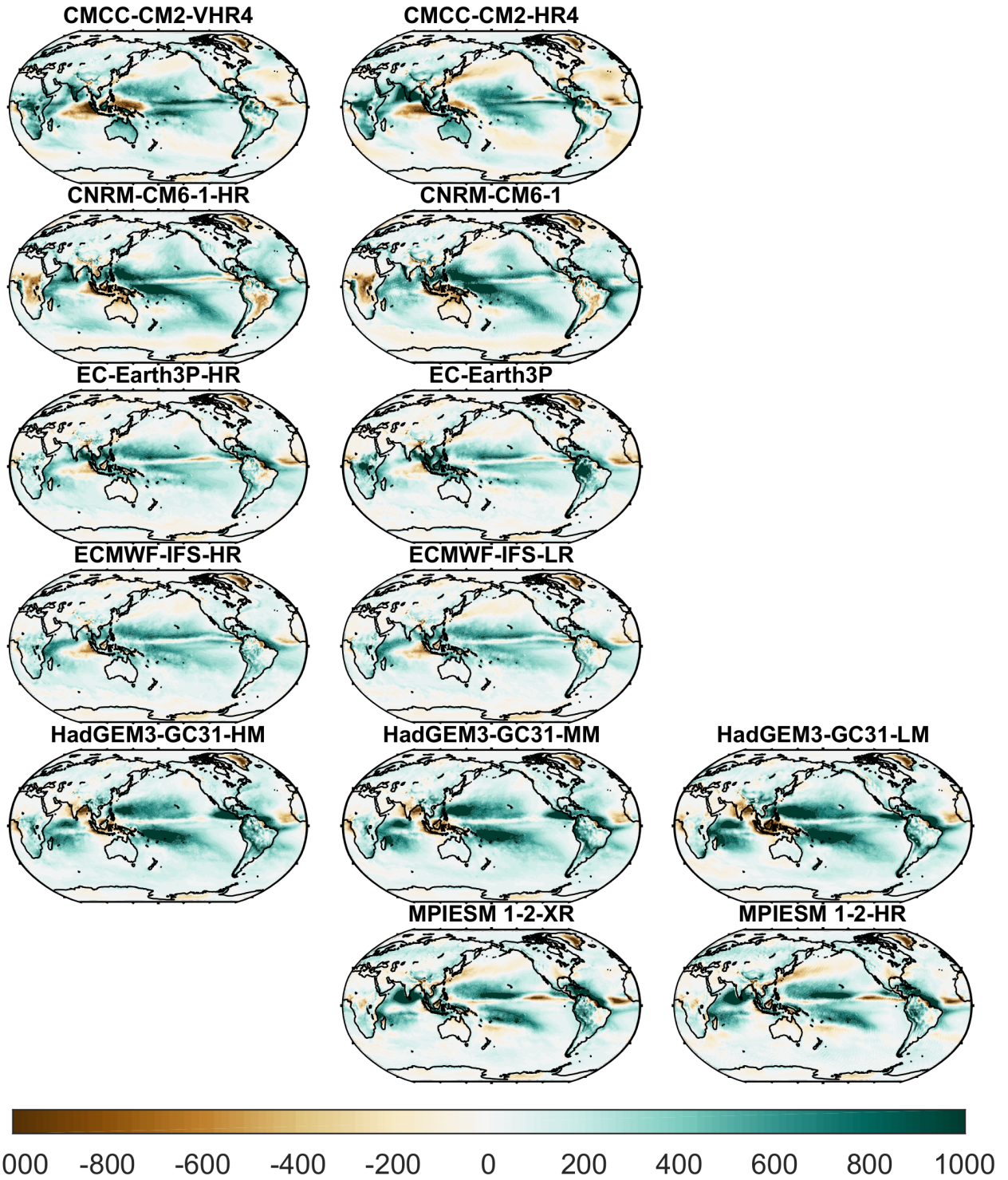
Figure 6. Bias (model minus observations) in total rainfall (unit: mm/year) in the models.

648

649
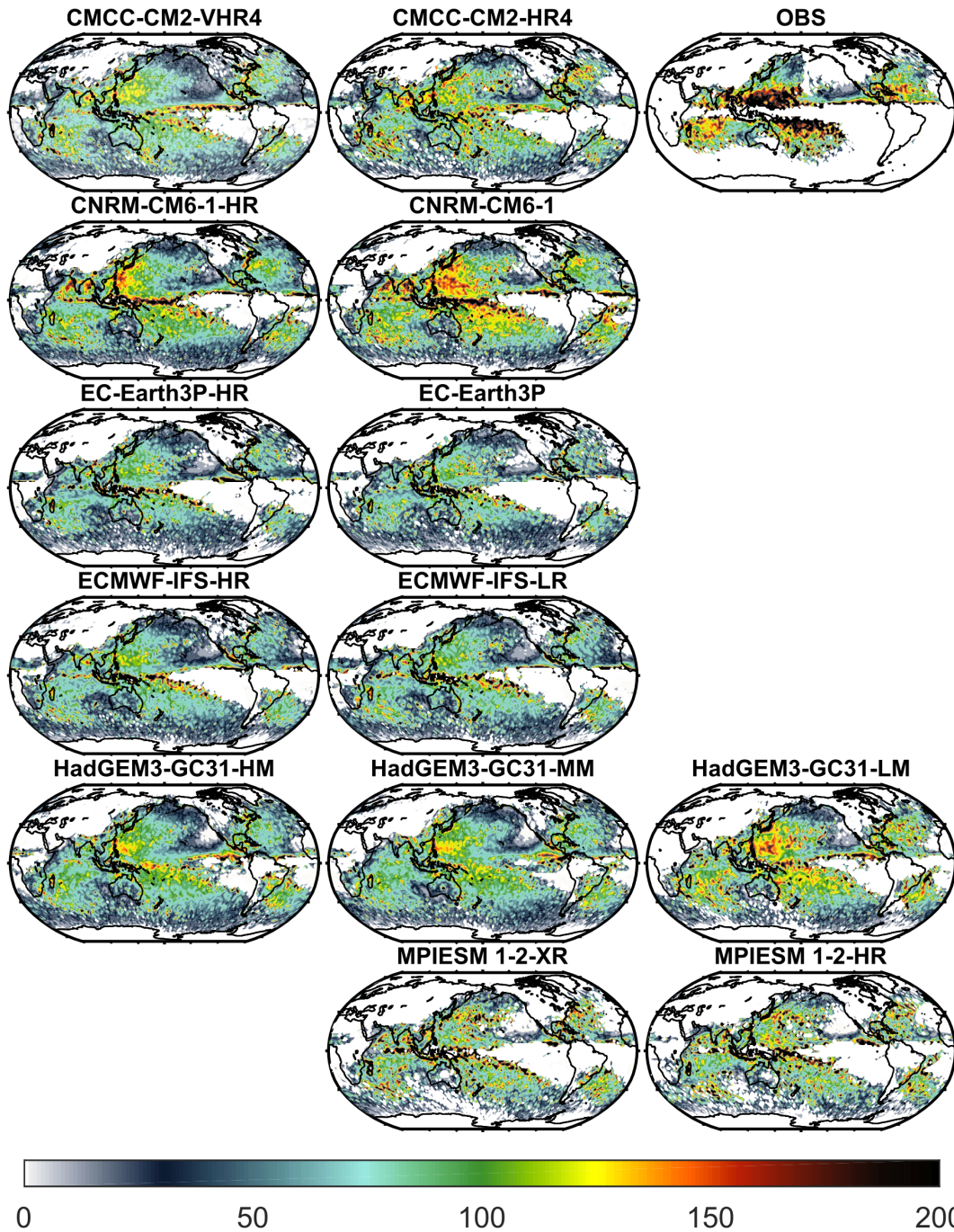
Figure 7. Average rainfall divided by TC track density (unit: mm) in observations and climate models archived in the PRIMAVERA Project. Average rainfall per TC track density represent the annual total TC rainfall divided by TC track density obtained by binning TC tracks into 2×2 spatial boxes.

654
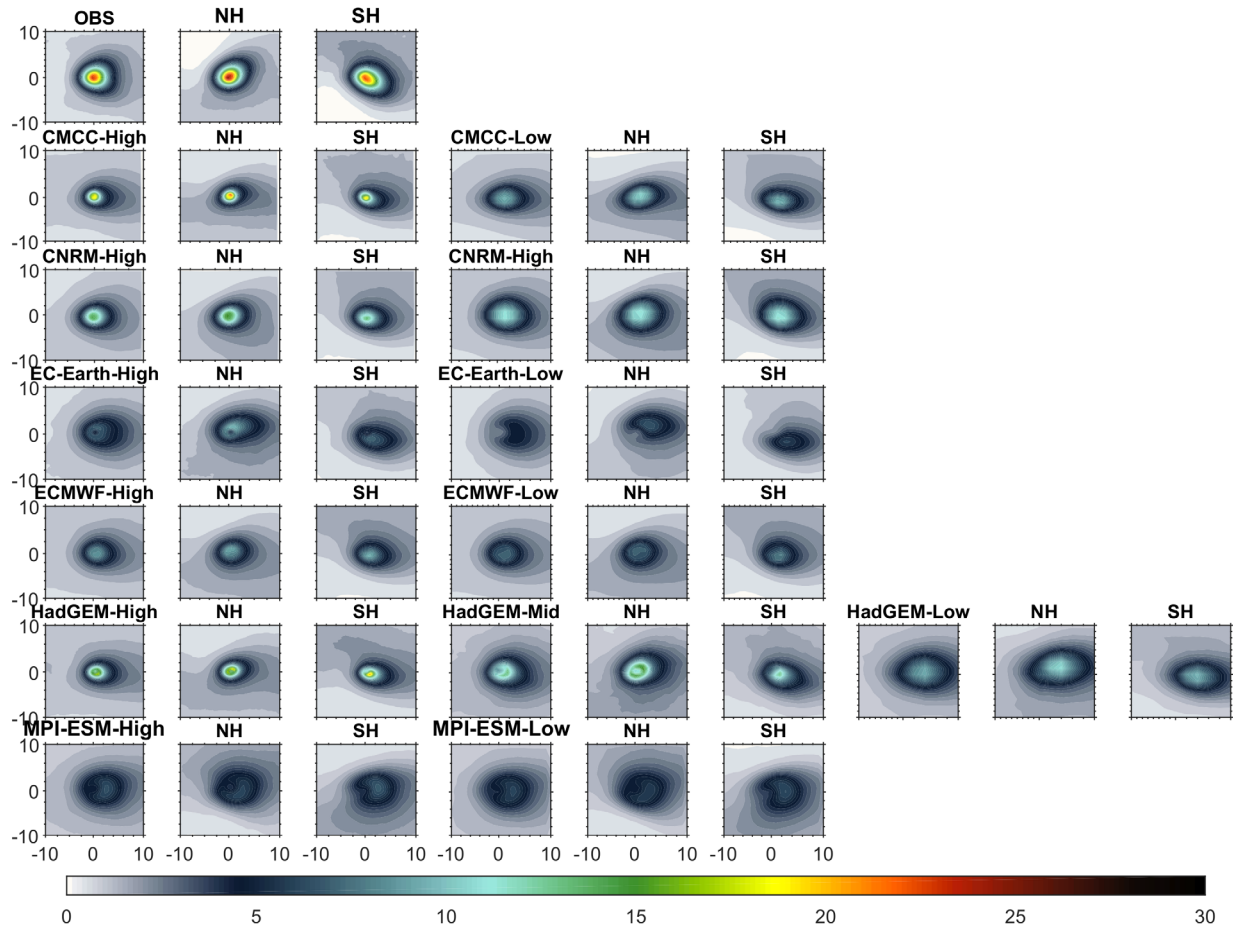
Figure 8. Composite 6-hour TC Rainfall (unit: mm) over the ocean & land in observations and climate models archived in the PRIMAVERA Project. The model resolution drops from left (columns 1-3) to right (columns 4-6 and 7-9). Every group of three columns represents the composite for all the storms, those in the northern hemisphere and those in the southern hemisphere.
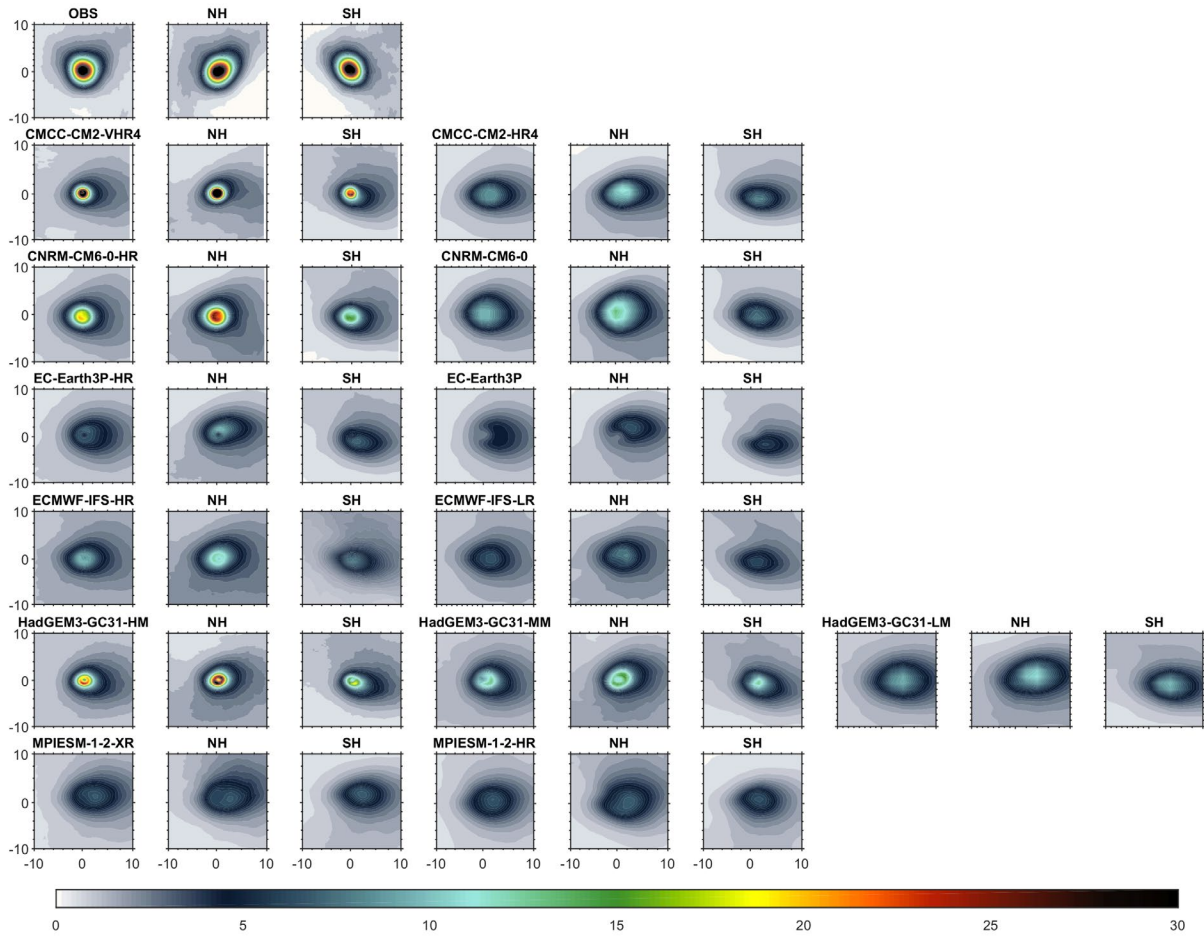
Figure 9. Composite 6-hour TC rainfall (unit: mm) across the 200 TCs with strongest intensity (sea level pressure) over the land and ocean in observations and climate models archived in the PRIMAVERA Project during 1980-2010. The model resolution drops from left (columns 1-3) to right (columns 4-6 and 7-9).
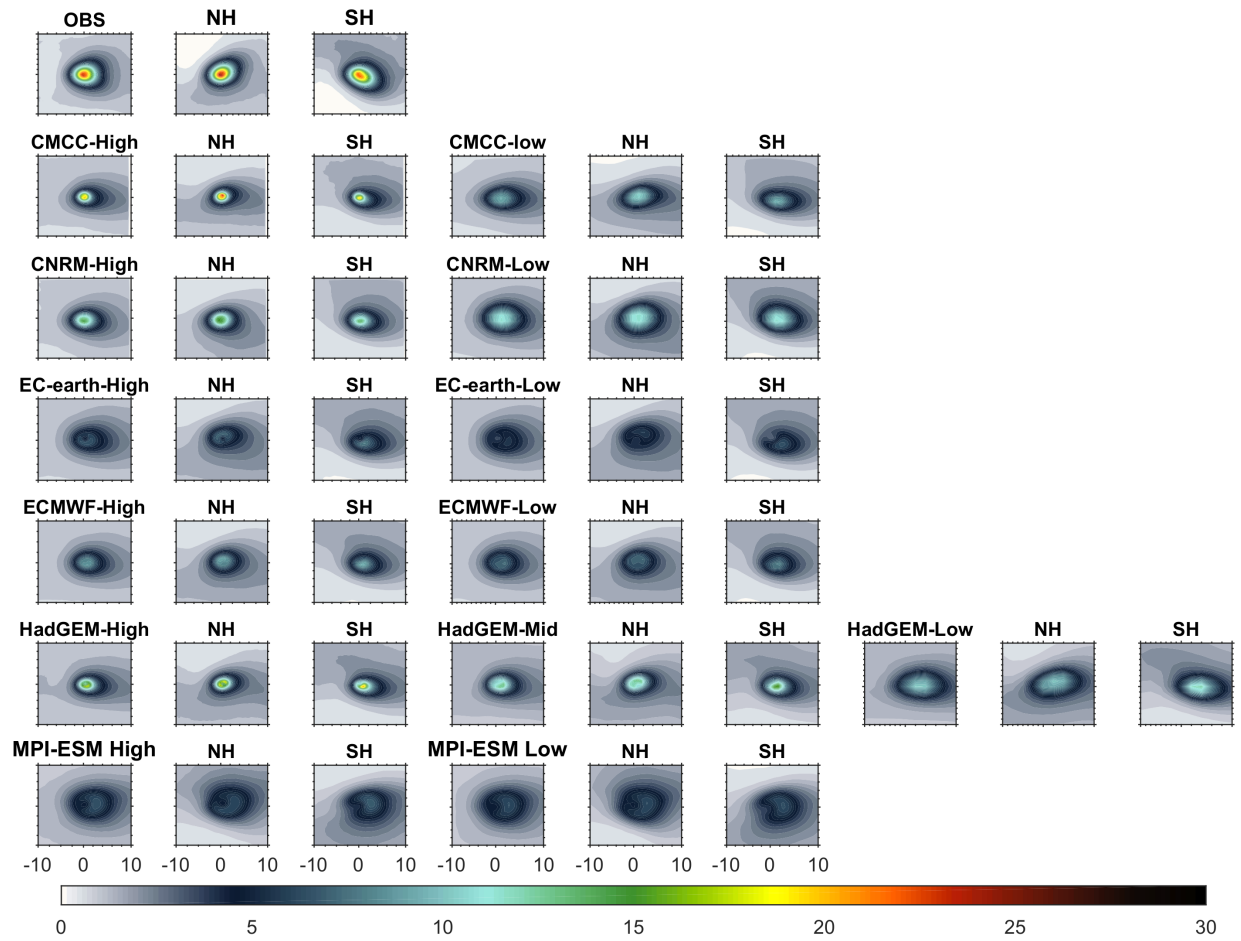
Figure 10. Same as Figure 8 but over ocean.

671
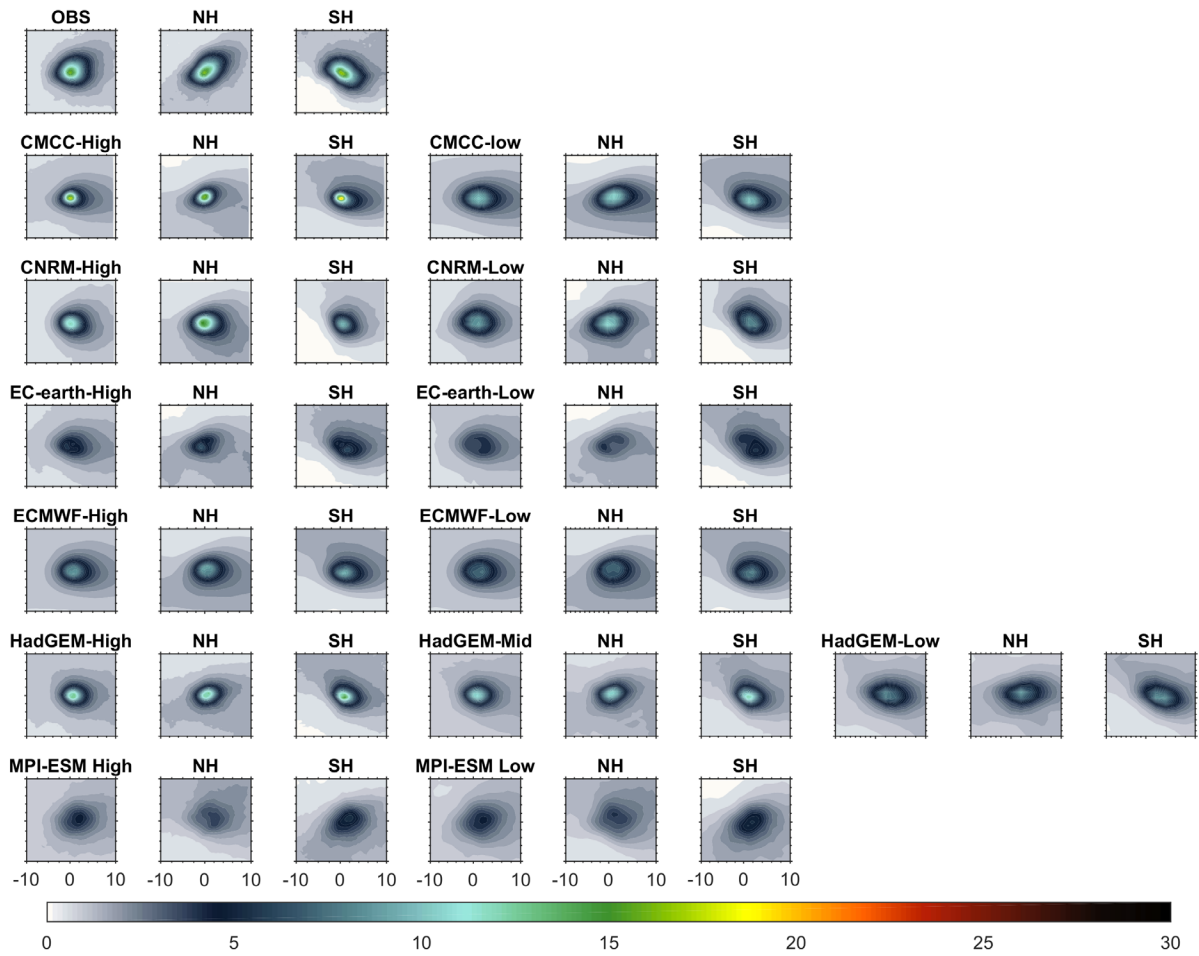
Figure 11. Same as Figure 8 but over land.

672

673

674

675

676
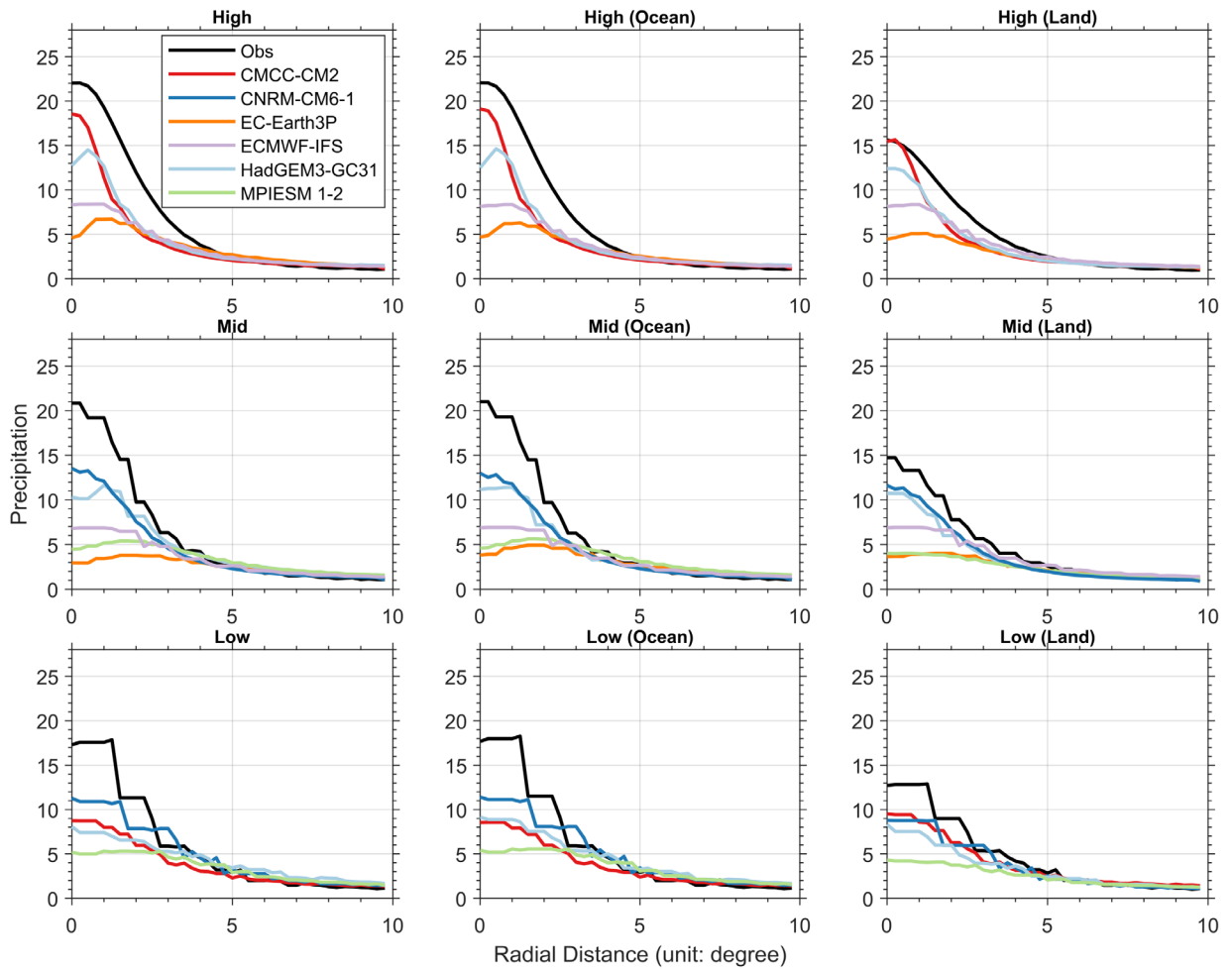
677   Figure 12. Radial profile of composite 6-hour TC rainfall (unit: mm) in observations and
678   models grouped into high-, mid-, and low-resolution climate models. The spatial resolution of
679   observed TC rainfall is re-gridded to each group (High, Mid and Low resolution) of the models.

680

681

34

682 Table 1. Spatial grids of the climate model outputs in high-, middle- and low-resolution groups
683 used in this study. While ECMWF IFS data provided to HighResMIP are based on a reduced-
684 resolution regular grid, the original ECMWF-IFS output uses the cubic octahedral reduced
685 Gaussian grid, with resolutions of Tco399 (~25 km) and Tco199 (~50 km) for the HR and LR
686 configurations, respectively.

Model	High	Middle/Medium	Low
CMCC-CM2	1152×768		288×192
CNRM-CM6-1		720×360	256×128
EC-Earth3P	1024×512	512×256	
ECMWF-IFS	720×361	360×181	
HadGEM3-GC313	1024×768	432×324	192×144
MPI-ESM1-2		768×384	384×192

687

688

689

690

691

692

693

694

695

696 Table 2 Definitions of basin boundaries

Basins	Boundary
Western North Pacific (WNP)	0-60°N, 100°E-180
Eastern North Pacific (ENP)	0-60°N, 180-100°W
North Atlantic (NA)	0-60°N, 100°W-0
North Indian Ocean (NI)	0-45°N, 45°E-100°E
South-West Indian Ocean (SI)	0-40°S, 0-90°E
South Pacific & Australia (SP)	0-40°S, 90°E-120°W
South Atlantic (SA)	0-60°S, 60°W-0

697

698

699

700

701

702 Table 3 Correlation between observed and simulated tropical cyclone rainfall across the globe
703 and in different basins.

	Globe	WNP	ENP	NA	NI	SI	SP
CMCC-CM2-VHR4	0.77	0.87	0.77	0.68	0.83	0.80	0.76
CMCC-CM2-HR4	0.54	0.62	0.59	0.41	0.77	0.80	0.61
CNRM-CM6-1-HR	0.80	0.94	0.29	0.80	0.70	0.84	0.79
CNRM-CM6-1	0.81	0.89	0.41	0.82	0.74	0.88	0.72
EC-Earth3P-HR	0.85	0.89	0.37	0.77	0.89	0.86	0.90
EC-Earth3P	0.83	0.85	0.33	0.78	0.92	0.88	0.89
ECMWF-IFS-HR	0.87	0.92	0.71	0.79	0.87	0.84	0.85
ECMWF-IFS-LR	0.86	0.92	0.66	0.80	0.88	0.81	0.85
HadGEM3-GC31-HM	0.83	0.94	0.74	0.71	0.62	0.86	0.78
HadGEM3-GC31-MM	0.83	0.93	0.71	0.71	0.70	0.85	0.76
HadGEM3-GC31-LM	0.83	0.94	0.69	0.75	0.76	0.86	0.71
MPIESM 1-2-XR	0.67	0.68	0.26	0.64	0.81	0.73	0.81
MPIESM 1-2-HR	0.71	0.76	0.13	0.75	0.91	0.74	0.82

704

705 Table 4 Root mean square error (unit: mm) between observed and simulated tropical cyclone
706 rainfall across the globe and in different basins.

	Globe	WNP	ENP	NA	NI	SI	SP
CMCC-CM2-VHR4	73.39	97.99	61.43	84.63	151.15	64.61	77.94
CMCC-CM2-HR4	79.44	152.37	14.90	80.66	140.61	83.06	74.72
CNRM-CM6-1-HR	95.27	136.22	27.57	46.58	280.06	61.12	67.15
CNRM-CM6-1	106.18	171.88	31.54	53.07	267.48	82.55	80.14
EC-Earth3P-HR	50.48	85.67	14.43	53.69	99.63	54.91	50.96
EC-Earth3P	54.26	125.33	13.08	51.90	40.53	51.50	42.83
ECMWF-IFS-HR	51.28	75.38	16.20	50.56	90.48	58.20	64.27
ECMWF-IFS-LR	49.17	75.97	15.91	44.59	93.09	62.63	61.00
HadGEM3-GC31-HM	129.29	159.11	59.40	161.02	75.63	151.65	143.76
HadGEM3-GC31-MM	130.32	173.13	56.98	151.07	68.51	145.72	147.59
HadGEM3-GC31-LM	76.46	96.64	25.58	62.46	45.38	70.04	96.37
MPIESM 1-2-XR	72.34	171.84	14.29	61.76	43.83	74.66	64.69
MPIESM 1-2-HR	69.57	167.61	14.15	57.32	31.24	72.98	61.12

707

708

709   Table 5 Correlation between observed and simulated tropical cyclone rainfall proportion across
710   the globe and in different basins.

	Globe	WNP	ENP	NA	NI	SI	SP
CMCC-CM2-VHR4	0.80	0.86	0.88	0.85	0.71	0.79	0.87
CMCC-CM2-HR4	0.65	0.72	0.71	0.64	0.67	0.79	0.86
CNRM-CM6-1-HR	0.71	0.92	0.55	0.75	0.64	0.85	0.86
CNRM-CM6-1	0.75	0.92	0.53	0.73	0.72	0.93	0.88
EC-Earth3P-HR	0.82	0.91	0.57	0.78	0.80	0.88	0.95
EC-Earth3P	0.81	0.90	0.53	0.72	0.87	0.89	0.95
ECMWF-IFS-HR	0.80	0.93	0.83	0.74	0.78	0.85	0.89
ECMWF-IFS-LR	0.79	0.92	0.79	0.70	0.80	0.82	0.91
HadGEM3-GC31-HM	0.86	0.93	0.78	0.87	0.84	0.88	0.83
HadGEM3-GC31-MM	0.85	0.92	0.71	0.86	0.80	0.88	0.82
HadGEM3-GC31-LM	0.79	0.94	0.67	0.81	0.64	0.90	0.69
MPIESM 1-2-XR	0.69	0.70	0.08	0.64	0.77	0.77	0.89
MPIESM 1-2-HR	0.73	0.77	-0.05	0.67	0.83	0.77	0.93

711

712

713   Table 6 Root mean square error (unit: %) between observed and simulated tropical cyclone
714   rainfall proportion across the globe and in different basins.

	Globe	WNP	ENP	NA	NI	SI	SP
CMCC-CM2-VHR4	5.10	5.90	3.41	5.32	9.66	7.93	6.43
CMCC-CM2-HR4	6.58	9.13	2.11	8.61	6.89	9.81	9.88
CNRM-CM6-1-HR	6.57	4.80	2.42	6.98	18.22	6.28	6.69
CNRM-CM6-1	6.26	4.85	2.50	6.97	16.71	4.66	6.14
EC-Earth3P-HR	4.80	6.20	2.41	6.70	7.95	6.47	4.18
EC-Earth3P	5.44	8.59	2.66	8.08	3.73	7.07	5.34
ECMWF-IFS-HR	4.99	4.70	1.77	6.78	8.36	7.26	5.79
ECMWF-IFS-LR	5.03	5.51	1.92	7.49	7.24	7.09	5.03
HadGEM3-GC31-HM	5.14	5.92	3.29	4.92	5.28	6.48	7.99
HadGEM3-GC31-MM	5.14	5.75	3.14	5.14	5.21	5.96	8.26
HadGEM3-GC31-LM	5.10	4.23	2.09	6.82	6.07	5.86	8.78
MPIESM 1-2-XR	6.87	10.79	2.86	9.43	4.82	9.46	9.41
MPIESM 1-2-HR	6.68	10.66	2.90	9.42	4.37	9.23	8.10

715

716

Tropical Cyclone Precipitation in the HighResMIP Atmosphere-only Experiments of the PRIMAVERA Project

Wei Zhang[1,2*], Gabriele Villarini[1], Enrico Scoccimarro[3], Malcolm Roberts[4], Pier Luigi Vidale[5], Benoıt Vanniere[5], Louis-Philippe Caron[6], Dian Putrasahan[7], Christopher Roberts[8], Retish Senan[8], and Marie-Pierre Moine[9]

[1] IIHR-Hydroscience & Engineering, The University of Iowa, Iowa City, Iowa, USA

[2] Department of Plants, Soils and Climate, Utah State University, Utah, USA

[3] Fondazione Centro Euro-Mediterraneo sui Cambiamenti Climatici, Bologna, Italy

[4] UK Meteorological Office, Exeter, UK

[5] National Centre for Atmospheric Science (NCAS), Department of Meteorology, University of Reading, Reading, UK

[6] Barcelona Supercomputing Center (BSC), Barcelona, Spain

[7] Max Planck Gesellschaft zur Foerderung der Wissenschaften E.V. (MPI-M), Hamburg, Germany

[8] European Centre for Medium-Range Weather Forecasts (ECMWF), Reading, UK

[9] Climat, Environnement, Couplages, Incertitudes (CECI), Universit´e de Toulouse, CNRS, Cerfacs, Toulouse, France

741 Table S1 Climatological frequencies of tropical cyclones (January-December, unit: mean
742 storms/yr) in the globe and different basins in observations and the climate models.

	Globe	NH	SH	WNP	ENP	NA	NI	SI	SP	SA
Observations	91.6	59.6	32	24.5	19.9	11.9	3.3	14.9	17.1	0
CMCC-CM2-VHR4	148.4	82.8	65.6	33.7	21.3	15.9	11.9	10.3	45.4	9.9
CMCC-CM2-HR4	83.6	48.1	35.5	20.1	7.3	11.4	9.3	6.5	24.1	4.9
CNRM-CM6-1-HR	163	84.8	78.2	40.1	11.3	18.9	14.5	15.6	52.1	10.5
CNRM-CM6-1	167.4	86	81.4	42	13.4	17.6	13	19.7	52	9.7
EC-Earth3P-HR	95.2	48.8	46.4	25	8.2	7.5	8.1	10.5	28.6	7.3
EC-Earth3P	72.7	31.8	40.9	17.2	4.9	4.8	4.9	8.5	25.4	7
ECMWF-IFS-HR	133.1	65.9	67.2	34.7	10.3	12.1	8.8	13	41	13.2
ECMWF-IFS-LR	117.5	58.1	59.4	30.4	9	9.6	9.1	12.3	36.3	10.8
HadGEM3-GC31-HM	206.6	99.7	106.9	43.3	23.6	25.5	7.3	23	69.8	14.1
HadGEM3-GC31-MM	215.4	104.7	110.7	47.3	25.1	24.8	7.5	23.8	73	13.9
HadGEM3-GC31-LM	138.4	63.3	75.1	34.9	12.9	12.3	3.2	16.1	49.7	9.3
MPIESM 1-2-XR	47.3	19.6	27.7	7.8	4.6	3.3	3.9	6	15.6	6.1
MPIESM 1-2-HR	46.9	20.5	26.4	8.6	3.9	4.2	3.8	6.6	15.7	4.1

743

744

745 Table S2 Correlation between observed and simulated tropical cyclone rainfall per TC across the
746 globe and in different basins.

	Globe	WNP	ENP	NA	NI	SI	SP
CMCC-CM2-VHR4	0.25	0.09	0.46	0.21	0.25	0.10	0.23
CMCC-CM2-HR4	0.18	0.08	0.22	0.08	0.20	0.09	0.19
CNRM-CM6-1-HR	0.28	0.19	0.46	0.19	0.32	0.03	0.11
CNRM-CM6-1	0.26	0.16	0.36	0.19	0.18	0.04	0.14
EC-Earth3P-HR	0.26	0.16	0.38	0.24	0.22	0.09	0.17
EC-Earth3P	0.28	0.19	0.34	0.23	0.28	0.07	0.27
ECMWF-IFS-HR	0.29	0.20	0.43	0.26	0.28	0.11	0.16
ECMWF-IFS-LR	0.30	0.16	0.47	0.24	0.36	0.09	0.19
HadGEM3-GC31-HM	0.28	0.17	0.38	0.24	0.27	0.18	0.29
HadGEM3-GC31-MM	0.26	0.17	0.47	0.14	0.36	0.11	0.12
HadGEM3-GC31-LM	0.21	0.15	0.50	0.10	0.16	0.02	0.07
MPIESM 1-2-XR	0.17	0.06	0.22	0.17	0.16	0.11	0.17
MPIESM 1-2-HR	0.23	0.11	0.36	0.22	0.26	0.10	0.24

747

748

749

750

751

752

Table S3 Root mean square error between observed and simulated tropical cyclone rainfall per
TC across the globe and in different basins.

	Globe	WNP	ENP	NA	NI	SI	SP
CMCC-CM2-VHR4	122.0	133.0	123.8	87.4	138.7	97.6	126.3
CMCC-CM2-HR4	126.5	133.8	139.1	101.2	137.5	103.3	125.8
CNRM-CM6-1-HR	118.7	128.0	122.0	81.0	131.4	95.3	129.0
CNRM-CM6-1	118.1	127.7	127.1	86.2	137.9	92.7	130.1
EC-Earth3P-HR	126.5	136.4	132.6	87.1	152.7	103.7	128.8
EC-Earth3P	126.8	136.3	143.4	93.3	145.8	102.5	126.0
ECMWF-IFS-HR	122.4	133.1	123.9	86.2	143.3	99.7	129.5
ECMWF-IFS-LR	122.1	133.6	121.6	87.8	137.8	98.7	127.9
HadGEM3-GC31-HM	120.9	130.7	126.8	82.0	148.8	93.4	122.6
HadGEM3-GC31-MM	121.7	130.1	122.4	88.9	141.4	94.8	130.4
HadGEM3-GC31-LM	122.5	128.7	117.0	93.3	151.8	100.8	135.9
MPIESM 1-2-XR	138.4	147.3	149.7	116.2	148.9	111.3	145.0
MPIESM 1-2-HR	129.2	144.3	123.0	91.4	141.5	110.7	138.3

755

756

Table S4 Root mean square error and correlation between observed and simulated tropical
cyclone rainfall across ocean and land.

	Cor (Ocean)	Cor (Land)	RMSE(Ocean)	RMSE(Land)
CMCC-CM2-VHR4	0.79	0.68	66.22	47.32
CMCC-CM2-HR4	0.57	0.51	76.33	36.06
CNRM-CM6-1-HR	0.83	0.67	84.74	64.69
CNRM-CM6-1	0.83	0.62	100.07	57.45
EC-Earth3P-HR	0.86	0.81	48.42	22.17
EC-Earth3P	0.83	0.78	53.15	19.15
ECMWF-IFS-HR	0.88	0.82	47.95	28.07
ECMWF-IFS-LR	0.87	0.83	46.61	24.76
HadGEM3-GC31-HM	0.83	0.79	126.41	48.80
HadGEM3-GC31-MM	0.83	0.80	128.95	40.77
HadGEM3-GC31-LM	0.84	0.83	76.46	18.41
MPIESM 1-2-XR	0.67	0.64	71.22	24.76
MPIESM 1-2-HR	0.72	0.66	68.45	24.08

759
760
761

762
763
764
765
766

767 Table S5 Root mean square error and correlation between observed and simulated tropical
768 cyclone rainfall proportion across ocean and land.
769

	Cor (Ocean)	Cor (Land)	RMSE(Ocean)	RMSE(Land)
CMCC-CM2-VHR4	0.83	0.69	4.62	3.25
CMCC-CM2-HR4	0.71	0.58	6.45	2.39
CNRM-CM6-1-HR	0.79	0.64	5.27	5.67
CNRM-CM6-1	0.80	0.64	5.42	4.71
EC-Earth3P-HR	0.85	0.74	4.50	2.52
EC-Earth3P	0.84	0.77	5.38	1.62
ECMWF-IFS-HR	0.84	0.71	4.51	3.22
ECMWF-IFS-LR	0.82	0.78	4.78	2.46
HadGEM3-GC31-HM	0.87	0.83	4.85	2.68
HadGEM3-GC31-MM	0.86	0.82	4.89	2.50
HadGEM3-GC31-LM	0.80	0.78	5.04	1.66
MPIESM 1-2-XR	0.70	0.72	6.85	1.86
MPIESM 1-2-HR	0.74	0.74	6.66	1.77

770
771
772
773

774 Table S6 Root mean square error and correlation between observed and simulated tropical
775 cyclone rainfall per TC across ocean and land.
776

	Cor (Ocean)	Cor (Land)	RMSE(Ocean)	RMSE(Land)
CMCC-CM2-VHR4	0.23	0.22	149.59	119.35
CMCC-CM2-HR4	0.16	0.11	153.68	130.84
CNRM-CM6-1-HR	0.29	0.25	144.20	120.22
CNRM-CM6-1	0.28	0.13	142.20	131.28
EC-Earth3P-HR	0.29	0.19	149.68	134.39
EC-Earth3P	0.25	0.20	157.39	136.33
ECMWF-IFS-HR	0.29	0.19	149.05	121.70
ECMWF-IFS-LR	0.31	0.26	146.64	123.05
HadGEM3-GC31-HM	0.31	0.18	146.65	126.26
HadGEM3-GC31-MM	0.30	0.13	146.91	129.38
HadGEM3-GC31-LM	0.25	0.04	144.65	136.30
MPIESM 1-2-XR	0.17	0.05	163.18	155.18
MPIESM 1-2-HR	0.20	0.17	161.12	145.98

777

778